

Hierarchical Enumeration Based on Skeletons of Ligancy 6 by Using Combined-Permutation Representations. Part 2. Prismane Derivatives

Shinsaku Fujita

Shonan Institute of Chemoinformatics and Mathematical Chemistry,

Kaneko 479-7 Ooimachi, Ashigara-Kami-Gun, Kanagawa-Ken,

258-0019 Japan

shinsaku.fujita@nifty.com

(Received April 4, 2017)

Abstract

Group hierarchy for characterizing a prismane skeleton with six substitution positions has been discussed by defining the point group (PG), the *RS*-stereoisomeric group (*RS*-SIG), the stereoisomeric group (SIG), and the isoskeletal group (ISG) successively as follows: PG D_{3h} (order 12) \subset *RS*-SIG $D_{3h\bar{\sigma}\hat{I}}$ (order 24) = SIG (the same as $D_{3h\bar{\sigma}\hat{I}}$) \subset ISG $S_{\sigma\hat{I}}^{[6]}$ (order 1440). On the basis of combined-permutation representations (S. Fujita, *MATCH Commun. Math. Comput. Chem.* **76** (2016) 379–400), Fujita's proligand method (S. Fujita, *Combinatorial Enumeration of Graphs, Three-Dimensional Structures, and Chemical Compounds*, University of Kragujevac, Faculty of Science, Kragujevac, 2013) is modulated and applied to the enumeration of prismane derivatives under the group hierarchy. A set of three ligand-inventory functions is introduced into cycle indices with chirality fittingness (CI-CFs) to give generating functions for the enumeration of 3D structures under PG and *RS*-SIG. On the other hand, a single ligand-inventory function is introduced into CI-CFs to give generating functions for the enumeration of 2D structures under SIG and ISG. The enumeration results are discussed systematically in terms of isomer-classification diagrams.

1 Introduction

Prismane (IUPAC name: tetracyclo[2.2.0.0^{2,6}.0^{3,5}]hexane) is called Ladenburg's benzene, because it was proposed in 1869 by Ladenburg [1] as a possible structure of benzene, which is a hydrocarbon with the molecular formula C₆H₆. Nowadays, Kekulé's benzene [2] is recognized as the correct structure of benzene. Prismane itself was synthesized as a tetracyclic compound in 1973 [3].

During the elucidation of the correct structure of benzene, it was examined whether or not a possible structure (Kekulé's benzene [2], Ladenburg's benzene [1], Dewar's benzene [4], or more) is capable of rationalizing the number of benzene derivatives with two or more substituents. For a historical description on the elucidation of the benzene structure, see Chapter 12 of [5].

The number of benzene derivatives has been systematically investigated in the first stage of Pólya's enumeration method [6–9]. The legacy of Pólya's paper [9] has been discussed by Read in its English translation [10], where the enumeration of benzene derivatives has been adopted as a typical example of the application of Pólya's enumeration method to chemical problems.

The comparison between a prismane skeleton and a benzene skeleton in terms of Pólya's enumeration method has been conducted by Pólya himself in Chapter 6 of [11], where the same cycle index (CI) has been assigned to both of the skeletons. The same CI stems from the implicit standpoint of Pólya's approach [11], in which the point group **D**_{3h} (order 12) for characterizing the prismane skeleton is interpreted as a permutation group, where rotations and reflections (containing roto reflections) are mixed up in terms of permutations. Note that the dihedral group **D**₆ (order 12) for characterizing the benzene skeleton consists of rotations only and is interpreted as the same permutation group. Pólya's theorem has been concluded to be deficient in the concept of sphericities, as discussed in a review of the author (Fujita) [12].

The concept of sphericities has originally been proposed to explain the behaviors of equivalence classes (orbits) during the development of the unit-subduced-cycle-index (USCI) approach proposed by the author (Fujita) [13, 14]. Fujita's USCI approach supports symmetry-itemized enumeration of 3D structures, where unit subduced cycle indices with chirality fittingness (USCI-CFs) are used to treat chiral proligands as well as achiral proligands. Among the four methods supported by Fujita's USCI approach, the fixed-

point-matrix (FPM) method and the partial-cycle-index (PCI) method have been applied to the symmetry-itemized enumeration of prismane derivatives [15].

The concept of *sphericities for orbits* has been extended into the concept of *sphericities for cycles*, which gives theoretical foundations to the proligand method proposed by the author (Fujita) [16, 17]. Fujita's proligand method supports gross enumeration of 3D structures, where cycle indices with chirality fittingness (CI-CFs) are used to treat chiral proligands as well as achiral proligands. The remaining task is the application of Fujita's proligand method to gross enumeration of prismanes, which will be discussed in the present article.

For the purpose of integrating chirality (geometric features of stereochemistry) and stereogenicity (stereoisomeric features of stereochemistry), the author (Fujita) has developed the stereoisogram approach [18–20], which is based on *RS*-stereoisomeric groups for mathematical treatments and on stereoisograms as their diagrammatic expressions. Fujita's stereoisogram approach has been applied to prismane derivatives [21].

During the above-mentioned investigations on Fujita's USCI approach [14, 22], Fujita's proligand method [17], and Fujita's stereoisogram approach [20], each ligand reflection is explicitly represented by an overbar to express the behaviors of chiral proligands as well as those of achiral proligands [22–24]. As a result, a reflection is totally represented by a permutation with an overbar (e.g., $\sigma_h \sim \overline{(1\ 4)(2\ 5)(3\ 6)}$), whereas a rotation and an *RS*-permutation are represented by permutations without an overbar (e.g., $\tilde{\sigma}_h \sim (1\ 4)(2\ 5)(3\ 6)$). However, this type of representations are unsuitable for practical computer-manipulation by such computer systems as GAP [25].

As computer-oriented representations suitable for practical calculations, combined-permutation representations (CPRs) have recently been developed by the author (Fujita) [26]. The CPRs have been used to treat point groups [26, 27] and *RS*-stereoisomeric groups [28]. For the purpose of gaining a wider outlook on computer-oriented representations, enumeration using such CPRs should be investigated by referring to the following group hierarchy:

$$\begin{aligned} \text{point groups (PG)} &\subseteq \text{RS-stereoisomeric groups (RS-SIG)} \\ &\subseteq \text{stereoisomeric groups (SIG)} \subseteq \text{isoskeletal groups (ISG)}, \quad (1) \end{aligned}$$

where each symbol \subseteq can be altered to represent a net subset (\subset) or an equality ($=$) in accord with a skeleton to be examined. Part 1 of this series has investigated enumeration

based on a cyclopropane skeleton of ligancy 6 by referring to Eq. 1, where there appear no equality symbols in Eq. 1. The next task assigned to Part 2 is systematic examination of a prismane skeleton of ligancy 6 by referring to the group hierarchy of Eq. 1, where there appears an equality symbol between *RS*-SIG and SIG.

2 Group hierarchy for prismane derivatives

2.1 Point groups for characterizing prismane derivatives

As shown in the left part of Figure 1, a prismane skeleton **1** belongs to the point group \mathbf{D}_{3h} (order 12), which has been also assigned to a cyclopropane skeleton in Part 1 of this series. The six positions of **1** construct an orbit (an equivalence class) controlled by the coset representation $(\mathbf{C}_s \setminus) \mathbf{D}_{3h}$, each element of which is represented by a permutation of degree 6. For the purpose of discriminating a reflection from a rotation, the expression of such a coset representation as $(\mathbf{C}_s \setminus) \mathbf{D}_{3h}$ has been devised (cf. [23, 24] and Chapter 6 of [22]) to be a permutation with an overbar for representing a reflection (e.g., $\sigma_h \sim \overline{(1\ 4)(2\ 5)(3\ 6)}$) in comparison with a permutation without an overbar for representing a rotation (e.g., $C_3 \sim (1\ 2\ 3)(4\ 5\ 6)$). In this article, the term *reflection* is used to mean rotoreflections (e.g., S_3 and S_3^2) as well as (pure) reflections.

The point group \mathbf{D}_{3h} exhibits the following coset decomposition:

$$\mathbf{D}_{3h} = \mathbf{D}_3 + \mathbf{D}_{3h}\sigma_h, \quad (2)$$

where the horizontal reflection σ_h is selected as a transversal. Then, the coset $\mathbf{D}_3I (= \mathbf{D}_3)$ contains six rotations (the upper-left part of Figure 1), while the other coset $\mathbf{D}_3\sigma_h$ contains six reflections (the lower-left part of Figure 1).

To treat a ligand reflection represented by an overbar, a mirror-permutation representation is introduced by considering the action on the domain $\chi = \{7, 8\}$. For example, the reflection $\sigma_h (\sim \overline{(1\ 4)(2\ 5)(3\ 6)})$ acts on the domain χ to give a 2-cycle (7 8). Thereby, a product of cycles (1 4)(2 5)(3 6)(7 8) is obtained by substituting a 2-cycle (7 8) for an overbar of $\overline{(1\ 4)(2\ 5)(3\ 6)}$. In the GAP system, the resulting product of cycles is expressed to be (1,4)(2,5)(3,6)(7,8) by the addition of commas.

On the other hand, a rotation (e.g., $C_3 \sim (1\ 2\ 3)(4\ 5\ 6)$) contained in the point group \mathbf{D}_{3h} acts on the domain χ to give a product of 1-cycles (7)(8). Thereby, a product of cycles with (7)(8) (e.g., (1 2 3)(4 5 6)(7)(8)) is obtained to show no ligand reflections (no

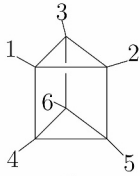
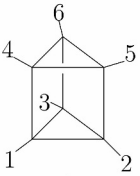
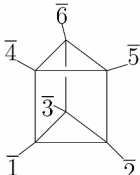
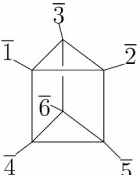
| | | | |
|---|--|--|--------------------------------|
| Stereoisomeric group \parallel RS-Stereoisomeric group $D_{3h\tilde{\sigma}\hat{I}}$ | | | |
| |  <p>1</p> |  <p>2</p> | |
| D_3 | | $D_{3\tilde{\sigma}h}$ | |
| I | (1)(2)(3)(4)(5)(6) | $\tilde{\sigma}_h$ | (1 4)(2 5)(3 6) b_3^3 |
| C_3 | (1 2 3)(4 5 6) | \tilde{S}_3 | (1 5 3 4 2 6) b_6 |
| C_3^2 | (1 3 2)(4 6 5) | \tilde{S}_3^2 | (1 6 2 4 3 5) b_6 |
| $C_{2(1)}$ | (1 4)(2 6)(3 5) | $\tilde{\sigma}_{v(1)}$ | (1)(2 3)(4)(5 6) $b_1^2 b_2^2$ |
| $C_{2(2)}$ | (1 6)(2 5)(3 4) | $\tilde{\sigma}_{v(2)}$ | (1 3)(2)(4 6)(5) $b_1^2 b_2^2$ |
| $C_{2(3)}$ | (1 5)(2 4)(3 6) | $\tilde{\sigma}_{v(3)}$ | (1 2)(3)(4 5)(6) $b_1^2 b_2^2$ |
| $D_3\sigma_h$ |  <p>1</p> |  <p>2</p> | |
| $D_3\hat{I}$ | | $D_3\hat{I}$ | |
| σ_h | (1 4)(2 5)(3 6) | \hat{I} | (1)(2)(3)(4)(5)(6) a_1^6 |
| S_3 | (1 5 3 4 2 6) | \hat{C}_3 | (1 2 3)(4 5 6) a_3^2 |
| S_3^2 | (1 6 2 4 3 5) | \hat{C}_3^2 | (1 3 2)(4 6 5) a_3^2 |
| $\sigma_{v(1)}$ | (1)(2 3)(4)(5 6) | $\hat{C}_{2(1)}$ | (1 4)(2 6)(3 5) c_3^2 |
| $\sigma_{v(2)}$ | (1 3)(2)(4 6)(5) | $\hat{C}_{2(2)}$ | (1 6)(2 5)(3 4) c_3^2 |
| $\sigma_{v(3)}$ | (1 2)(3)(4 5)(6) | $\hat{C}_{2(3)}$ | (1 5)(2 4)(3 6) c_3^2 |

Figure 1. RS-Stereoisomeric group $D_{3h\tilde{\sigma}\hat{I}}$ ($= D_{3h} + D_{3h}\tilde{\sigma}_h$) derived from a coset representation of D_{3h} for characterizing a prismane skeleton. The RS-Stereoisomeric group $D_{3h\tilde{\sigma}\hat{I}}$ is coincident with the corresponding stereoisomeric group in the case of the prismane skeleton.

overbars). The resulting product of cycles is expressed to be $(1,2,3)(4,5,6)$, where 1-cycles are omitted according to the mathematical convention adopted by the GAP system.

The procedures described above are applied to the rotations and the reflections of D_{3h} . This means the combination of the coset representation $(C_s \setminus) D_{3h}$ (or $D_{3h} (/ C_s)$) with a mirror-permutation representation $(\{(7)(8), (7\ 8)\})$. The resulting representation is designated by the symbol $P_{D_{3h}}^{(X_X)}(D_{3h})$, which is called *the combined-permutation representation* (CPR), as described in Part I of this series. The CPR $P_{D_{3h}}^{(X_X)}(D_{3h})$ can be regarded as a permutation group of degree 8 ($= 6 + 2$), which is suitable for handling by the GAP system.

By relying on the combined-permutation representations (CPRs), the coset decomposition represented by Eq. 2 is practically calculated by the GAP system as follows:

```
gap> D3 := Group([(1,2,3)(4,5,6), (1,4)(2,6)(3,5)]);
Group([ (1,2,3)(4,5,6), (1,4)(2,6)(3,5) ])
gap> D3h := Group([(2,3)(5,6)(7,8), (1,2)(4,5)(7,8), (1,4)(2,5)(3,6)(7,8)]);
Group([ (2,3)(5,6)(7,8), (1,2)(4,5)(7,8), (1,4)(2,5)(3,6)(7,8) ])
gap> CosetDecomposition(D3h,D3);
[ [ () , (1,2,3)(4,5,6), (1,3,2)(4,6,5), (1,4)(2,6)(3,5), (1,5)(2,4)(3,6), (1,6)(2,5)(3,4) ],
  [ (1,4)(2,5)(3,6)(7,8), (1,5,3,4,2,6)(7,8), (1,6,2,4,3,5)(7,8), (2,3)(5,6)(7,8), (1,2)(4,5)(7,8),
    (1,3)(4,6)(7,8) ] ]
gap> Elements(RightTransversal(D3h,D3));
[ () , (1,4)(2,5)(3,6)(7,8) ]
```

Note that the CPRs $P_{D_3}^{(X_X)}(D_3)$ and $P_{D_{3h}}^{(X_X)}(D_{3h})$ for the point groups D_3 and D_{3h} are generated from the respective sets of generators described in the GAP function `Group` (cf. Part I of this series). The GAP function `CosetDecomposition` gives the coset decomposition in the form of a GAP list, in which an inner pair of square brackets is a list of elements contained in each coset. Thus, the first inner pair of square brackets contains six permutations with omitted 1-cycles $((7)(8))$, while the second inner pair contains six permutations with an explicit 2-cycle $(7,8)$. The GAP function `RightTransversal` generates a list of transversals (I and σ_h).

2.2 *RS*-stereoisomeric group for prismane derivatives

2.2.1 Reflections and *RS*-permutations for prismane derivatives

The top row of Figure 2 illustrates the effect of a horizontal reflection σ_h applied to the numbered skeleton **1** of prismane, where a shadowed triangle shows a mirror plane for specifying σ_h ($\sim \overline{(1\ 4)(2\ 5)(3\ 6)}$). Thereby, the reflection σ_h converts the numbered skeleton **1** into the corresponding mirror-numbered skeleton $\bar{\mathbf{1}}$. Each locant number with an overbar (i.e., $\bar{1}, \bar{2}, \dots$, or $\bar{6}$) indicates a ligand reflection, where the corresponding

position accommodates a proligand after the alternation of its chirality sense.

Fujita's stereoisogram approach has defined an *RS*-permutation by starting from a reflection contained in a point group [20]. For example, an *RS*-permutation $\tilde{\sigma}_h$ ($\sim (1\ 4)(2\ 5)(3\ 6)$) is defined by omitting ligand reflections from the corresponding reflection σ_h ($\sim \overline{(1\ 4)(2\ 5)(3\ 6)}$). The effect of the resulting *RS*-permutation $\tilde{\sigma}_h$ is illustrated in the bottom row of Figure 2, where the numbered skeleton **1** is converted into the corresponding *RS*-numbered skeleton **2**. The *RS*-permutation $\tilde{\sigma}_h$ can be interpreted by the intervention of a graph $\mathbf{1}_g$, where the lift of the outer triangle (attached by 4, 5, and 6) gives the *RS*-numbered skeleton **2** without accompanying ligand reflections.

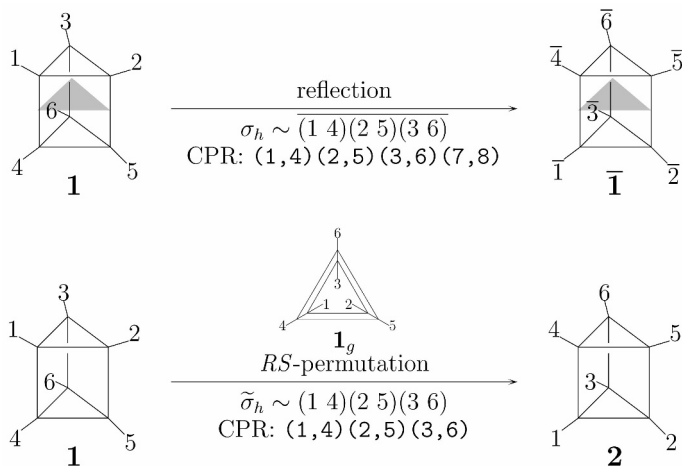


Figure 2. Reflections and *RS*-permutations applied to a prismane skeleton. The plane containing a shadowed triangle is a mirror plane for specifying a horizontal reflection σ_h . The acronym CPR denotes *combined-permutation representation*.

In a similar way to the rotation C_3 described above, the *RS*-permutation $\tilde{\sigma}_h$ ($\sim (1\ 4)(2\ 5)(3\ 6)$) acts on the domain χ to give a product of 1-cycles (7)(8). Thereby, a product of cycles $(1\ 4)(2\ 5)(3\ 6)(7)(8)$ is obtained to show no ligand reflections (no overbars). The resulting product of cycles is expressed to be $(1, 4)(2, 5)(3, 6)$, where 1-cycles are omitted according to the criteria of the GAP system.

2.2.2 Construction of *RS*-stereoisomeric group for prismane derivatives

In part 1 of this series, the *RS*-stereoisomeric group $D_{3h\tilde{\sigma}\hat{I}}$ (Figure 1) has been constructed by considering the following coset decomposition:

$$D_{3h\tilde{\sigma}\hat{I}} = D_{3h} + D_{3h}\tilde{\sigma}_h. \quad (3)$$

As shown in Table 1 of Part 1 of this series, however, the GAP system has resulted in the formation of the following D3hsI:

```
D3hsI := Group([ (7,8), (2,3)(5,6), (1,2)(4,5), (1,4)(2,5)(3,6) ]);
```

This means that the resulting set of generators for D3hsI has been obtained in accord with the following coset decomposition:

$$D_{3h\tilde{\sigma}\hat{I}} = D_{3\tilde{\sigma}} + D_{3\tilde{\sigma}}\hat{I}, \quad (4)$$

because the first element (7,8) in the source list of D3hsI corresponds to a net ligand reflection \hat{I} ($= \sigma_h\tilde{\sigma}_h \sim \overline{(1)(2)(3)(4)(5)(6)}$) and because the *RS*-permutation group $D_{3\tilde{\sigma}}$ is represented as follow:

$$D_{3\tilde{\sigma}} = D_3 + D_3\tilde{\sigma}_h. \quad (5)$$

Thus, the elements of $D_{3\tilde{\sigma}}$ shown in the upper-left and upper-right parts of Figure 1 is generated by the following generators:

```
D3s := Group([ (2,3)(5,6), (1,2)(4,5), (1,4)(2,5)(3,6) ]);
```

This set of generators for the *RS*-permutation group $D_{3\tilde{\sigma}}$ (D3s) has appeared in the source list of D3hsI. Thus, the addition of (7,8) to the set of generators for D3s results in the formation of the set of generators for D3hsI.

Because D_{3h} in Eq. 3 and $D_{3\tilde{\sigma}}$ in Eq. 4 contain a common subgroup D_3 , the following coset decomposition is obtained:

$$D_{3h\tilde{\sigma}\hat{I}} = D_3 + D_3\sigma_h + D_3\tilde{\sigma}_h + D_3\hat{I} \quad (6)$$

This coset decomposition is confirmed by the GAP system as follows:

```
gap> D3 := Group([(1,2,3)(4,5,6), (1,4)(2,6)(3,5)]);
gap> D3hsI := Group([(7,8), (2,3)(5,6), (1,2)(4,5), (1,4)(2,5)(3,6)]);
gap> CosetDecomposition(D3hsI,D3);
[ [ () , (1,2,3)(4,5,6), (1,3,2)(4,6,5), (1,4)(2,6)(3,5), (1,5)(2,4)(3,6), (1,6)(2,5)(3,4) ],
  [ (2,3)(5,6), (1,3)(4,6), (1,2)(4,5), (1,4)(2,5)(3,6), (1,6,2,4,3,5), (1,5,3,4,2,6) ],
  [ (7,8), (1,2,3)(4,5,6)(7,8), (1,3,2)(4,6,5)(7,8), (1,4)(2,6)(3,5)(7,8), (1,5)(2,4)(3,6)(7,8),
    (1,6)(2,5)(3,4)(7,8) ],
  [ (2,3)(5,6)(7,8), (1,3)(4,6)(7,8), (1,2)(4,5)(7,8), (1,4)(2,5)(3,6)(7,8), (1,6,2,4,3,5)(7,8),
    (1,5,3,4,2,6)(7,8) ] ]
gap> List(RightTransversal(D3hsI,D3), i->CanonicalRightCosetElement(D3,i));
[ () , (2,3)(5,6), (7,8), (2,3)(5,6)(7,8) ]
```

The four inner lists surrounded separately by a pair of square brackets in the output of the GAP function `CosetDecomposition` correspond to the four cosets appearing in Eq. 6. These cosets and the transversals of this source list (the output of `RightTransversal`) actually correspond to the following coset decomposition:

$$\mathbf{D}_{3h\tilde{\sigma}\hat{I}} = \mathbf{D}_3 + \mathbf{D}_3\tilde{\sigma}_{v(1)} + \mathbf{D}_3\hat{I} + \mathbf{D}_3\sigma_{v(1)}, \quad (7)$$

which is equivalent with Eq. 6 because $\mathbf{D}_3\tilde{\sigma}_{v(1)} = \mathbf{D}_3\tilde{\sigma}_h$ and $\mathbf{D}_3\sigma_{v(1)} = \mathbf{D}_3\sigma_h$.

2.3 Stereoisomeric group and isoskeletal group for a prismane skeleton

2.3.1 Stereoisomeric group equal to *RS*-stereoisomeric group

As for the group hierarchy of the prismane skeleton **1**, the stereoisomeric group becomes the same as the *RS*-stereoisomeric group $\mathbf{D}_{3h\tilde{\sigma}\hat{I}}$ (order 24). It follows that the general group hierarchy represented by Eq. 1 is reduced to the following scheme:

$$\begin{aligned} &\text{point group (PG) } \mathbf{D}_{3h} \subset \textit{RS}\text{-stereoisomeric group (RS-SIG) } \mathbf{D}_{3h\tilde{\sigma}\hat{I}} \\ &= \text{stereoisomeric group (SIG) } \subset \text{isoskeletal group (ISG) } \mathbf{S}_{\sigma\hat{I}}^{[6]}. \end{aligned} \quad (8)$$

Although the same group $\mathbf{D}_{3h\tilde{\sigma}\hat{I}}$ is assigned both to *RS*-stereoisomerism and to stereoisomerism during discussions on the group hierarchy of the prismane skeleton **1**, the former *RS*-stereoisomerism is concerned with 3D structures, while the latter stereoisomerism is concerned with 2D structures (graphs). In spite of the same group, the difference between *RS*-stereoisomerism and stereoisomerism results in the selection of different ligand-inventory functions, as discussed below in detail.

2.4 Isoskeletal group for prismane derivatives

In place of the isoskeletal group $\tilde{\mathbf{D}}_{3h\tilde{\sigma}\hat{I}}$ (order 1440) defined in Part 1 of this series, we use the reflective symmetric group $\mathbf{S}_{\sigma\hat{I}}^{[6]}$ (order 1440, the combined representation as a group: **S6sI**) for the purpose of characterizing the isoskeletomerism of the prismane skeleton **1**. This is because there are many transversals for the construction of $\tilde{\mathbf{D}}_{3h\tilde{\sigma}\hat{I}}$ (order 1440) from the *RS*-stereoisomeric group $\mathbf{D}_{3h\tilde{\sigma}\hat{I}}$ (**D3hsI**, order 24).

Under isoskeletomerism, the six positions of **1** can be permuted freely to give the symmetric group of degree 6 ($\mathbf{S}^{[6]}$, order $6! = 720$), where each element of $\mathbf{S}^{[6]}$ is regarded

as an operation for converting a numbered skeleton into another numbered skeleton. Then, ligand reflections are considered to generate the reflective symmetric group $\mathbf{S}_{\sigma\hat{I}}^{[6]}$ as follows:

$$\mathbf{S}_{\sigma\hat{I}}^{[6]} = \mathbf{S}^{[6]} + \mathbf{S}^{[6]}\hat{I}, \quad (9)$$

which is here equalized to the isoskeletal group $\widetilde{\mathbf{D}}_{3h\sigma\hat{I}}$. The set of generators for $\mathbf{S}^{[6]}$ is found to be $[(1,2,3,4,5,6), (1,2)]$ and the ligand reflection $\hat{I} (\sim \overline{(1)(2)(3)(4)(5)(6)})$ is expressed to be (7,8). They are combined to give $[(1,2,3,4,5,6), (1,2), (7,8)]$ as the set of generators for $\mathbf{S}_{\sigma\hat{I}}^{[6]}$.

The point group \mathbf{D}_3 and the RS -permutation group $\mathbf{D}_{3\bar{\sigma}}$ are regarded as the subgroups of the symmetric group $\mathbf{S}^{[6]}$. The point group \mathbf{D}_{3h} (D3h) and the RS -stereoisomeric group $\mathbf{D}_{3h\sigma\hat{I}}$ (D3hsI) are regarded as the subgroups of the reflective symmetric group $\mathbf{S}_{\sigma\hat{I}}^{[6]}$ (S6sI). The transversals of the coset decomposition of $\mathbf{S}_{\sigma\hat{I}}^{[6]}$ (S6sI, order 1440) by $\mathbf{D}_{3h\sigma\hat{I}}$ (D3hsI, order 24) are calculated as follows:

```
gap> D3hsI := Group([(7,8), (2,3)(5,6), (1,2)(4,5), (1,4)(2,5)(3,6)]);
gap> Size(D3hsI);
24
gap> S6sI := Group([(1,2,3,4,5,6), (1,2), (7,8)]);
gap> Size(S6sI);
1440
gap> List(RightTransversal(S6sI,D3hsI), i->CanonicalRightCosetElement(D3hsI,i));
[ (), (5,6), (4,5), (4,5,6), (4,6,5), (4,6), (3,4), (3,4)(5,6), (3,4,5), (3,4,5,6), (3,4,6,5), (3,4,6),
(3,5,4), (3,5,6,4), (3,5), (3,5,6), (3,5)(4,6), (3,5,4,6), (3,6,5,4), (3,6,4), (3,6,5), (3,6),
(3,6,4,5), (3,6)(4,5), (2,3,4), (2,3,4)(5,6), (2,3,4,5), (2,3,4,5,6), (2,3,4,6,5), (2,3,4,6),
(2,3,5,4), (2,3,5,6,4), (2,3,5), (2,3,5,6), (2,3,5)(4,6), (2,3,5,4,6), (2,3,6,5,4), (2,3,6,4),
(2,3,6,5), (2,3,6), (2,3,6,4,5), (2,3,6)(4,5), (2,4)(3,5), (2,4)(3,5,6), (2,4,3,5), (2,4,3,5,6),
(2,4,6,3,5), (2,4,6)(3,5), (2,4)(3,6,5), (2,4)(3,6), (2,4,3,6,5), (2,4,3,6), (2,4,5)(3,6),
(2,4,5,3,6), (2,5,3,6,4), (2,5,4)(3,6), (2,5)(3,6,4), (2,5,4,3,6), (2,5)(3,6), (2,5,3,6) ]
gap> Size(RightTransversal(S6sI,D3hsI));
60
```

There appear 60 transversals, each of which contains no reflection (no 2-cycle (7,8)). The 60 transversals construct the coset decomposition of $\mathbf{S}_{\sigma\hat{I}}^{[6]}$ (S6sI, order 1440) by $\mathbf{D}_{3h\sigma\hat{I}}$ (D3hsI, order 24) as follows:

$$\mathbf{S}_{\sigma\hat{I}}^{[6]} = \mathbf{D}_{3h\sigma\hat{I}} + \mathbf{D}_{3h\sigma\hat{I}}\widetilde{\sigma}_{56} + \mathbf{D}_{3h\sigma\hat{I}}\widetilde{\sigma}_{45} + \mathbf{D}_{3h\sigma\hat{I}}\widetilde{\sigma}_{456} + \cdots, \quad (10)$$

which satisfies $24 \times 60 = 1440$, where such symbols as $\widetilde{\sigma}_{56}$ represent operations corresponding to such transversals as (5,6) shown in the above source list. Obviously, the right-hand side of Eq. 10 can be adopted as an alternative formulation for constructing the isoskeletal group $\widetilde{\mathbf{D}}_{3h\sigma\hat{I}}$, if we follow the procedure described in Table 2 (cf. Eq. 10) of Part 1 of this series.

3 Hierarchical enumeration of prismane derivatives

The symmetry-itemized enumeration of prismane derivatives has been conducted by means of the fixed-point-matrix (FPM) method and the partial-cycle-index (PCI) method of Fujita's USCI approach [15]. Fujita's stereoisogram approach has been applied qualitatively to prismane derivatives by using the *RS*-stereoisomeric group $D_{3h\bar{\sigma}\bar{\tau}}$. In this article, Fujita's proligand method using cycle indices with chirality fittingness (CI-CFs) [16, 17, 29, 30] is extended to support hierarchical enumeration of prismane derivatives.

3.1 Calculation of CI-CFs

Cycle indices with chirality fittingness (CI-CFs) for point groups in Fujita's proligand method [16, 17, 29, 30] can be extended to support group hierarchy, where they are manually calculated from the products of sphericity indices (PSIs), which are in turn calculated by the examination of the cycle structures of the respective elements. For example, Figure 1 lists the PSIs of respective elements, which are calculated from the corresponding cycle structures by assigning a sphericity index (SI) b_d to each hemispheric d -cycle, an SI a_d to each homospheric d -cycle (d : odd), and an SI c_d to an enantiospheric d -cycle (d : even). The PSIs for $D_{3h\bar{\sigma}\bar{\tau}}$ are summed up and divided by the order $|D_{3h\bar{\sigma}\bar{\tau}}|$ ($= 24$) so as to give the following CI-CF:

$$\text{CI-CF}(D_{3h\bar{\sigma}\bar{\tau}}, \$_d) = \frac{1}{24} (b_1^6 + 3b_1^2b_2^2 + 4b_2^3 + 2b_3^2 + 2b_6 + a_1^6 + 3a_1^2c_2^2 + 4c_2^3 + 2a_3^2 + 2c_6), \quad (11)$$

where the symbol $\$_d$ indicates b_d , a_d , or c_d .

The manual calculation of the CI-CF described in the preceding paragraph can be systematically conducted by using the CPR [26] and the GAP function `CalcConjClassCICF` developed previously [27]. Thus, the CI-CF shown in Eq. 11 is obtained as follows:

```
gap> Read("c:/fujita0/fujita2017/prismane-GAP/calc-GAP/CICFgenCC.gapfunc");
gap> D3hsI := Group([(7,8), (2,3)(5,6), (1,2)(4,5), (1,4)(2,5)(3,6)]);
gap> Print("D3hsI:=", D3hsI, "\n");
D3hsI := Group( [ (7,8), (2,3)(5,6), (1,2)(4,5), (1,4)(2,5)(3,6) ] )
gap> Print("Order:=", Size(D3hsI), "\n");
Order := 24
gap> Print("CICF_D3hsI:=", CalcConjClassCICF(D3hsI, 6, 8), "\n");
CICF_D3hsI := 1/24*b_1^6+1/24*a_1^6+1/8*b_1^2*b_2^2+1/8*a_1^2*c_2^2+1/6*b_2^3
+1/6*c_2^3+1/12*b_3^2+1/12*a_3^2+1/12*b_6+1/12*c_6
```

Note that the GAP function `CalcConjClassCICF` is stored in the file `CICFgenCC.gapfunc`, which is placed in a directory named appropriately as above. The file `CICFgenCC.gapfunc` for calculating CI-CFs is loaded by the GAP function `Read`. The calculated CI-CF

Table 1. CI-CFs for Characterizing a Prismane Skeleton

| group | Group due to a list of generators, order, CI-CF |
|--|---|
| D_3 (point group) | D3 := Group([(1,2,3)(4,5,6), (1,4)(2,6)(3,5)]) Order := 6 CICF_D3 := 1/6*b_1^6+1/2*b_2^3+1/3*b_3^2 |
| D_{3h} (point group) | D3h := Group([(2,3)(5,6)(7,8), (1,2)(4,5)(7,8), (1,4)(2,5)(3,6)(7,8)]) Order := 12 CICF_D3h := 1/12*b_1^6+1/4*a_1^2*c_2^2+1/4*b_2^3+1/12*c_2^3+1/6*b_3^2+1/6*c_6 |
| $D_{3h\bar{\sigma}\bar{\Gamma}}$ (<i>RS</i> -stereo- isomeric group = stereoisomeric group) | D3hSI := Group([(7,8), (2,3)(5,6), (1,2)(4,5), (1,4)(2,5)(3,6)]) Order := 24 CICF_D3hSI := 1/24*b_1^6+1/24*a_1^6+1/8*b_1^2*b_2^2+1/8*a_1^2*c_2^2+1/6*b_2^3 +1/6*c_2^3+1/12*b_3^2+1/12*a_3^2+1/12*c_6 +1/12*b_6 |
| $S_{\sigma\bar{\Gamma}}^{[6]} = \tilde{D}_{3h\bar{\sigma}\bar{\Gamma}}$ (isoskeletal group) | S6sI := Group([(1,2,3,4,5,6), (1,2), (7,8)]) Order := 1440 CICF_S6sI := 1/1440*b_1^6+1/1440*a_1^6+1/96*b_1^4*b_2+1/96*a_1^4*c_2 +1/36*b_1^3*b_3+1/32*b_1^2*b_2^2+1/36*a_1^3*a_3+1/32*a_1^2*c_2^2 +1/16*b_1^2*b_4+1/12*b_1*b_3*b_2+1/96*b_2^3+1/16*a_1^2*c_4 +1/12*a_1*c_2*a_3+1/96*c_2^3+1/10*b_1*b_5+1/36*b_3^2+1/16*b_2*b_4 +1/10*a_1*a_5+1/16*c_2*c_4+1/36*a_3^2+1/12*c_6+1/12*b_6 |

(CICF_D3hSI) is identical with the manual result shown in Eq. 11. An asterisk * in the output of CICF_D3hSI indicates multiplication, so that the output 1/24*b_1^6, for example, means the term $\frac{1}{24}b_1^6$.

The output at the next line of each `gap>` prompt is taken up to print the $D_{3h\bar{\sigma}\bar{\Gamma}}$ -part of Table 1. Table 1 also lists the CI-CFs of the other groups, which are calculated in a similar way to the CI-CF of $D_{3h\bar{\sigma}\bar{\Gamma}}$. These results concerning the prismane skeleton **1** are consistent with the data concerning a cyclopropane skeleton (Table 3 of Part 1 of this series) except that the *RS*-stereoisomeric group is equal to the stereoisomeric group.

3.2 Enumerations under the point groups and under the *RS*-stereoisomeric group

3.2.1 Ligand-inventory functions for 3D enumeration

According to Fujita's proligand method [16, 17, 29, 30], enumerations under the point groups (D_3 and D_{3h}) and under *RS*-stereoisomeric group ($D_{3h\bar{\sigma}\bar{\Gamma}}$) are concerned with 3D structures, where proligands for enumerating prismane derivatives are selected from the following ligand inventory:

$$\mathbf{L}_{3D} = \{H, A, B, C, D, V; p, \bar{p}, q, \bar{q}, r, \bar{r}, s, \bar{s}, t, \bar{t}, u, \bar{u}\}, \quad (12)$$

where the uppercase letters H, A, B, C, D, and V represent achiral proligands, while a pair of lowercase letters p/\bar{p} , q/\bar{q} , r/\bar{r} , s/\bar{s} , t/\bar{t} , or u/\bar{u} represents an enantiomeric pair of chiral proligands in isolation (when detached).

A d -cycle accommodates d proligands selected from the ligand inventory (Eq. 12) in accord with the chirality fittingness (CF) due to the sphericity of the d -cycle, where a homospheric d -cycle is characterized by the SI a_d , an enantiospheric d -cycle is characterized by the SI c_d , and a hemispheric d -cycle is characterized by the SI b_d . The mode of accommodation in the d -cycle is determined by the following set of ligand-inventory functions:

$$a_d = H^d + A^d + B^d + C^d + D^d + V^d \quad (13)$$

$$c_d = H^d + A^d + B^d + C^d + D^d + V^d + 2p^{d/2}\bar{p}^{d/2} + 2q^{d/2}\bar{q}^{d/2} + 2r^{d/2}\bar{r}^{d/2} + 2s^{d/2}\bar{s}^{d/2} + 2t^{d/2}\bar{t}^{d/2} + 2u^{d/2}\bar{u}^{d/2} \quad (14)$$

$$b_d = H^d + A^d + B^d + C^d + D^d + V^d + p^d + \bar{p}^d + q^d + \bar{q}^d + r^d + \bar{r}^d + s^d + \bar{s}^d + t^d + \bar{t}^d + u^d + \bar{u}^d. \quad (15)$$

For the purpose of hierarchical enumeration, the ligand-inventory functions (Eqs. 13–15) are transformed into the following ligand-inventory functions for 3D enumeration by putting $\ddot{p} = p = \bar{p}$, $\ddot{q} = q = \bar{q}$, and so on:

$$a_d = H^d + A^d + B^d + C^d + D^d + V^d \quad (16)$$

$$c_d = H^d + A^d + B^d + C^d + D^d + V^d + 2\ddot{p}^d + 2\ddot{q}^d + 2\ddot{r}^d + 2\ddot{s}^d + 2\ddot{t}^d + 2\ddot{u}^d \quad (17)$$

$$b_d = H^d + A^d + B^d + C^d + D^d + V^d + 2\ddot{p}^d + 2\ddot{q}^d + 2\ddot{r}^d + 2\ddot{s}^d + 2\ddot{t}^d + 2\ddot{u}^d. \quad (18)$$

It should be noted that the substitution of $\ddot{p} = p = \bar{p}$ for deriving Eqs. 16–18 does not mean the degeneration of p/\bar{p} into a single graph. In other words, the distinction due to the SIs (a_d , c_d , and b_d) is maintained during the 3D enumeration, even though the symbol \ddot{p} is used to bundle p and \bar{p} .

3.2.2 Generating functions for point groups and *RS*-stereoisomeric groups

Suppose that the six positions of the prismane skeleton **1** accommodate a set of six proligands selected from the ligand inventory \mathbf{L}_{3D} (Eq. 12). Let the symbol $T_{(D_3)\ddot{\theta}}$ be the number of prismane derivatives with the weight $W_{\ddot{\theta}}$ under the action of the point group D_3 . Let the symbol $B_{(D_{3h})\ddot{\theta}}$ be the number of pairs of enantiomeric prismane derivatives

with the weight $W_{\tilde{\theta}}$ under the action of the point group \mathbf{D}_{3h} . The numbers $T_{(\mathbf{D}_3)\tilde{\theta}}$ and $B_{(\mathbf{D}_{3h})\tilde{\theta}}$ appear as the coefficients of the respective weights $W_{\tilde{\theta}}$ in the following generating functions:

$$\sum_{\tilde{\theta}} T_{(\mathbf{D}_3)\tilde{\theta}} W_{\tilde{\theta}} = \text{CI-CF}(\mathbf{D}_3, b_d) \Big|_{\text{Eq. 18}}, \quad (19)$$

$$\sum_{\tilde{\theta}} B_{(\mathbf{D}_{3h})\tilde{\theta}} W_{\tilde{\theta}} = \text{CI-CF}(\mathbf{D}_{3h}, \mathbb{S}_d) \Big|_{\text{Eqs. 16-18}}, \quad (20)$$

where the symbol $|_{\text{Eq. 18}}$ or $|_{\text{Eqs. 16-18}}$ means the introduction of the respective ligand-inventory function(s) into CI-CF(\mathbf{D}_3, b_d) (CICF_D3 in Table 1) or CI-CF($\mathbf{D}_{3h}, \mathbb{S}_d$) (CICF_D3h in Table 1).

Similarly, let the symbol $B_{(\mathbf{D}_{3h\tilde{\sigma}\tilde{\tau}})\tilde{\theta}}$ be the number of quadruplets of *RS*-stereoisomeric prismane derivatives with the weight $W_{\tilde{\theta}}$ under the action of the *RS*-stereoisomeric group $\mathbf{D}_{3h\tilde{\sigma}\tilde{\tau}}$. The number $B_{(\mathbf{D}_{3h\tilde{\sigma}\tilde{\tau}})\tilde{\theta}}$ appear as the coefficient of the weight $W_{\tilde{\theta}}$ in the following generating function:

$$\sum_{\tilde{\theta}} B_{(\mathbf{D}_{3h\tilde{\sigma}\tilde{\tau}})\tilde{\theta}} W_{\tilde{\theta}} = \text{CI-CF}(\mathbf{D}_{3h\tilde{\sigma}\tilde{\tau}}, \mathbb{S}_d) \Big|_{\text{Eqs. 16-18}}, \quad (21)$$

which is obtained by introducing the same set of ligand-inventory functions (Eqs. 16–18) into CI-CF($\mathbf{D}_{3h\tilde{\sigma}\tilde{\tau}}, \mathbb{S}_d$) (CICF_D3hsI in Table 1).

The weight $W_{\tilde{\theta}}$ in Eqs. 19–21 is calculated to be $H^h A^a B^b C^c D^d V^v \check{p}^{\check{p}} \check{q}^{\check{q}} \check{r}^{\check{r}} \check{s}^{\check{s}} \check{t}^{\check{t}} \check{u}^{\check{u}}$, where the powers satisfy the following equation:

$$h + a + b + c + d + v + \check{p} + \check{q} + \check{r} + \check{s} + \check{t} + \check{u} = 6. \quad (22)$$

The weight $W_{\tilde{\theta}}$ is represented by the partition $[\check{\theta}]$ as follows:

$$[\check{\theta}] = [h, a, b, c, d, v, \check{p}, \check{q}, \check{r}, \check{s}, \check{t}, \check{u}], \quad (23)$$

which satisfies $h \geq a \geq b \geq c \geq d \geq v$; and $\check{p} \geq \check{q} \geq \check{r} \geq \check{s} \geq \check{u} \geq \check{t}$, because respective terms appear symmetrically in such generating functions as Eqs. 19–21.

3.3 Enumerations under the stereoisomeric group and under the isoskeletal group

3.3.1 A single ligand-inventory function for graph enumeration

Suppose that a pair of p/\bar{p} , q/\bar{q} , r/\bar{r} , s/\bar{s} , t/\bar{t} , or u/\bar{u} degenerates into an single graph (2D structure), i.e., \check{p} , \check{q} , \check{r} , \check{s} , \check{t} , or \check{u} , during discussions on stereoisomers and isoskeletonomers.

Then, the ligand inventory \mathbf{L}_{3D} (Eq. 12) is transformed into the following ligand inventory for graph enumeration:

$$\mathbf{L}_{2D} = \{H, A, B, C, D, V; \check{p}, \check{q}, \check{r}, \check{s}, \check{t}, \check{u}\}. \quad (24)$$

A set of six 2D-entities (graphs) selected from \mathbf{L}_{2D} is placed on the prismane skeleton $\mathbf{1}$, so that a single ligand-inventory function for graph enumeration is obtained as follows:

$$a_d = c_d = b_d = H^d + A^d + B^d + C^d + D^d + V^d + \check{p}^d + \check{q}^d + \check{r}^d + \check{s}^d + \check{t}^d + \check{u}^d. \quad (25)$$

Note that the symbol \check{p} (\dots , or \check{u}) in Eq. 25 denotes a 2D-entity selected from \mathbf{L}_{2D} (Eq. 24), whereas the symbol \bar{p} (\dots , or \bar{u}) in Eqs. 16–18 is used to denote p and \bar{p} (\dots , or u and \bar{u}) separately under the same name \check{p} (\dots , or \check{u}).

3.3.2 Calculation of generating functions for stereoisomeric groups and isoskeletal groups

Because the stereoisomeric group for characterizing the prismane skeleton $\mathbf{1}$ is coincident with the *RS*-stereoisomeric group $\mathbf{D}_{3h\hat{\sigma}\hat{\tau}}$, the CI-CF represented by CI-CF($\mathbf{D}_{3h\hat{\sigma}\hat{\tau}}$, \mathbb{S}_d) (CICF_D3hsI) shown in Table 1 is used to enumerate prismane derivatives under stereoisomerism. Let the symbol $\tilde{B}_{(\mathbf{D}_{3h\hat{\sigma}\hat{\tau}})\check{\theta}}$ be the number of sets of stereoisomeric prismane derivatives with the weight $W_{\check{\theta}}$. The ligand-inventory function (Eq. 25) is introduced into CI-CF($\mathbf{D}_{3h\hat{\sigma}\hat{\tau}}$, \mathbb{S}_d) (CICF_D3hsI) shown in Table 1. Thereby, the following generating function is obtained:

$$\sum_{\check{\theta}} \tilde{B}_{(\mathbf{D}_{3h\hat{\sigma}\hat{\tau}})\check{\theta}} W_{\check{\theta}} = \text{CI-CF}(\mathbf{D}_{3h\hat{\sigma}\hat{\tau}}, \mathbb{S}_d) \Big|_{\text{Eq. 25}}. \quad (26)$$

Let the symbol $B_{(\mathbf{S}_{\sigma\hat{\tau}}^{[6]})\check{\theta}}$ be the number of sets of isoskeletal prismane derivatives with the weight $W_{\check{\theta}}$. The ligand-inventory function (Eq. 25) is introduced into CI-CF($\mathbf{S}_{\sigma\hat{\tau}}^{[6]}$, \mathbb{S}_d) (CICF_S6sI) shown in Table 1. Thereby, the following generating function is obtained:

$$\sum_{\check{\theta}} B_{(\mathbf{S}_{\sigma\hat{\tau}}^{[6]})\check{\theta}} W_{\check{\theta}} = \text{CI-CF}(\mathbf{S}_{\sigma\hat{\tau}}^{[6]}, \mathbb{S}_d) \Big|_{\text{Eq. 25}}. \quad (27)$$

3.4 Results of enumeration

3.4.1 GAP-calculation of generating functions

The generating functions shown in Eqs. 19, 20, 21, 26, and 27 are practically calculated by writing the GAP codes. The coefficients of the weight $W_{\check{\theta}}$, which are extracted from

the generating functions in a similar way to Appendix A of Part 1 of this series, are listed in tabular forms, where the group hierarchy is taken into consideration. Because the set of ligand-inventory functions (Eqs. 16–18) is used, the $T_{(D_3)\tilde{\theta}}$ -column (due to Eq. 19), the $B_{(D_{3h})\tilde{\theta}}$ -column (due to Eq. 20), and the $B_{(D_{3h\bar{\sigma}\hat{\Gamma}})\tilde{\theta}}$ -column (due to 21) are concerned with 3D structures,

Although the same CI-CF as the *RS*-stereoisomeric group $D_{3h\bar{\sigma}\hat{\Gamma}}$ is used, the $\tilde{B}_{(D_{3h\bar{\sigma}\hat{\Gamma}})\tilde{\theta}}$ -column (due to Eq. 26) is concerned with stereoisomers as graphs, because of the single ligand-inventory function (Eq. 25). The $B_{(S_{\sigma\hat{\Gamma}}^{[6]})\tilde{\theta}}$ -column (due to Eq. 27) is concerned with isoskeletonomers as graphs because the single ligand-inventory function (Eq. 25) is used.

3.4.2 Prismane derivatives with achiral proligands

Table 2 shows the hierarchical enumeration of prismane derivatives with achiral proligands and no chiral proligands. According to the definition of Eq. 23, the six integers at the first part of each partition ($[\tilde{\theta}]_1$ - $[\tilde{\theta}]_{11}$) are concerned with achiral proligands, while the six integers (all zero values) at the next part are concerned with chiral proligands.

Table 2. Hierarchical Enumeration of Prismane Derivatives with Achiral Proligands and No Chiral Proligands

| partition | numbers of prismane derivatives under respective groups | | | | |
|---|--|--|--|--|--|
| | $T_{(D_3)\tilde{\theta}}$ (Eq. 19) | $B_{(D_{3h})\tilde{\theta}}$ (Eq. 20) | $B_{(D_{3h\bar{\sigma}\hat{\Gamma}})\tilde{\theta}}$ (Eq. 21) | $\tilde{B}_{(D_{3h\bar{\sigma}\hat{\Gamma}})\tilde{\theta}}$ (Eq. 26) | $B_{(S_{\sigma\hat{\Gamma}}^{[6]})\tilde{\theta}}$ (Eq. 27) |
| | Eqs. 16–18 | | | Eq. 25 | |
| $[\tilde{\theta}]_1 = [6, 0, 0, 0, 0, 0, 0, 0, 0, 0, 0]$ | 1 | 1 | 1 | 1 | 1 |
| $[\tilde{\theta}]_2 = [5, 1, 0, 0, 0, 0, 0, 0, 0, 0, 0]$ | 1 | 1 | 1 | 1 | 1 |
| $[\tilde{\theta}]_3 = [4, 2, 0, 0, 0, 0, 0, 0, 0, 0, 0]$ | 4 | 3 | 3 | 3 | 1 |
| $[\tilde{\theta}]_4 = [4, 1, 1, 0, 0, 0, 0, 0, 0, 0, 0]$ | 5 | 3 | 3 | 3 | 1 |
| $[\tilde{\theta}]_5 = [3, 3, 0, 0, 0, 0, 0, 0, 0, 0, 0]$ | 4 | 3 | 3 | 3 | 1 |
| $[\tilde{\theta}]_6 = [3, 2, 1, 0, 0, 0, 0, 0, 0, 0, 0]$ | 10 | 6 | 6 | 6 | 1 |
| $[\tilde{\theta}]_7 = [3, 1, 1, 1, 0, 0, 0, 0, 0, 0, 0]$ | 20 | 10 | 10 | 10 | 1 |
| $[\tilde{\theta}]_8 = [2, 2, 2, 0, 0, 0, 0, 0, 0, 0, 0]$ | 18 | 11 | 11 | 11 | 1 |
| $[\tilde{\theta}]_9 = [2, 2, 1, 1, 0, 0, 0, 0, 0, 0, 0]$ | 30 | 16 | 16 | 16 | 1 |
| $[\tilde{\theta}]_{10} = [2, 1, 1, 1, 1, 0, 0, 0, 0, 0, 0]$ | 60 | 30 | 30 | 30 | 1 |
| $[\tilde{\theta}]_{11} = [1, 1, 1, 1, 1, 1, 0, 0, 0, 0, 0]$ | 120 | 60 | 60 | 60 | 1 |

The $[\tilde{\theta}]_3$ -row of Table 2 lists the numbers of prismane derivatives with the composition H^4A^2 under the respective groups. Note that the expression of the composition H^4A^2 stems from the weight $W_{\tilde{\theta}}$, so that it has no contribution of the six skeletal carbon atoms

of the prismane skeleton. Thus, if the proligand A represents an atom (e.g., Cl), the composition H^4A^2 corresponds to a molecular formula $C_6H_4A_2$ (e.g., $C_6H_4Cl_2$). To confirm these numbers, the following functions are applied to the prismane skeleton **1** shown in Figure 1.

$$f_1 : f_1(1) = f_1(5) = A; f_1(2) = f_1(3) = f_1(4) = f_1(6) = H, \quad (28)$$

$$f_2 : f_2(1) = f_2(2) = A; f_2(3) = f_2(4) = f_2(5) = f_2(6) = H, \quad (29)$$

$$f_3 : f_3(1) = f_3(4) = A; f_3(2) = f_3(3) = f_3(5) = f_3(6) = H, \quad (30)$$

By applying the function f_1 to **1** as a reference, there appears a prismane derivative **3** shown in Figure 3. Thereby, the four skeletons shown in Figure 1 totally generate a type-I stereoisogram, as shown in the upper-left part of Figure 3. This type-I stereoisogram consists of a pair of enantiomers $[\mathbf{3} \overline{\mathbf{3}}]$. The function f_2 generates a type-IV stereoisogram (the upper-right part of Figure 3), where the quadruplet of *RS*-stereoisomers degenerates into a single achiral prismane derivative $[\mathbf{5}]$. The function f_3 generates another type-IV stereoisogram (the bottom of Figure 3), where the quadruplet of *RS*-stereoisomers again degenerates into a single achiral prismane derivative $[\mathbf{7}]$.

It follows that the three functions (Eqs. 28–29) generate the three quadruplets of *RS*-stereoisomers (Figure 3). The stereoisograms of Figure 3 are consistent with Figures 7 and 8 of a previous article [21]. These three quadruplets can be expressed by such simplified schemes as $(\mathbf{3} \overline{\mathbf{3}})_{\text{I}}$, $(\mathbf{5})_{\text{IV}}$, and $(\mathbf{7})_{\text{IV}}$, which are inequivalent to one another under the *RS*-stereoisomeric group $D_{3h\overline{\sigma}\overline{\tau}}$. Each quadruplet of *RS*-stereoisomers is counted once under $D_{3h\overline{\sigma}\overline{\tau}}$. This result is consistent with the value 3 at the intersection between the $[\check{\theta}]_3$ -row and the $B_{(D_{3h\overline{\sigma}\overline{\tau}})\check{\theta}}$ -column in Table 2.

Each of the three stereoisograms shown in Figure 3 contains one pair of (self-)enantiomers, i.e., $[\mathbf{3} \overline{\mathbf{3}}]$ (a pair of enantiomers), $[\mathbf{5}]$ (a pair of self-enantiomers as an achiral prismane derivative), and $[\mathbf{7}]$ (a pair of self-enantiomers as an achiral prismane derivative), where a pair of square brackets indicates a pair of (self-)enantiomers. Hence, there appear three pairs of (self-)enantiomers under the action of the point group D_{3h} . This result is consistent with the value 3 at the intersection between the $[\check{\theta}]_3$ -row and the $B_{(D_{3h})\check{\theta}}$ -column in Table 2, because each pair of (self-)enantiomers is counted once under the point group D_{3h} .

The presence of four prismane derivatives, i.e., $\mathbf{3}, \overline{\mathbf{3}}, \mathbf{5}, \mathbf{7}$, is consistent with the value 4 at the intersection between the $[\check{\theta}]_3$ -row and the $T_{(D_3)\check{\theta}}$ -column in Table 2.

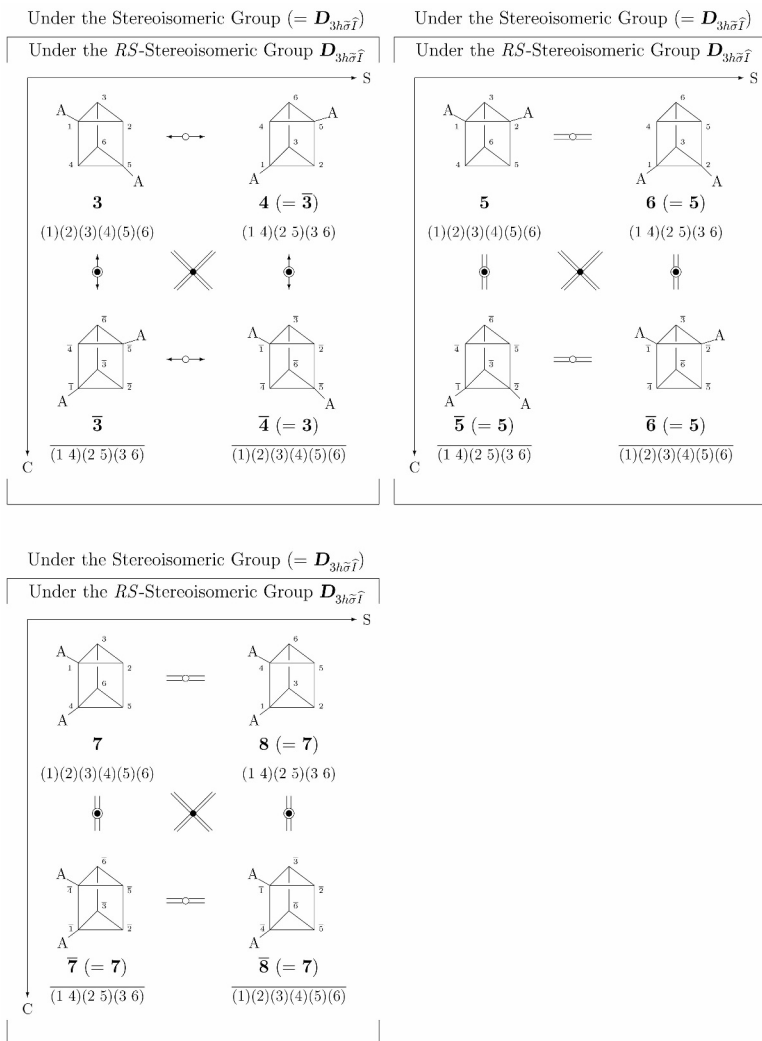


Figure 3. Type-I and two type-IV stereoisograms for characterizing prismane derivatives with composition H^4A^2 . Hydrogens are omitted. Each stereoisogram contains a quadruplet of *RS*-stereoisomers, which is counted once under the *RS*-stereoisomeric group $D_{3h\bar{\sigma}\hat{\Gamma}}$.

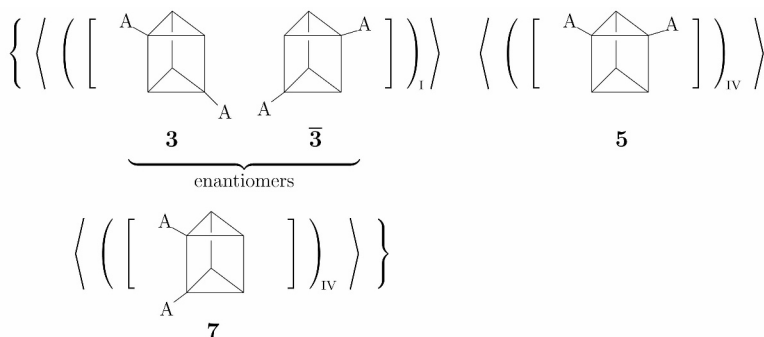


Figure 4. Isomer-classification diagram for prismanes with the composition H^4A^2 .

Table 2 is concerned with prismane derivatives with achiral proligands. As a result, the values under the RS -stereoisomeric group are equal to those under the stereoisomeric group, as found in the $B_{(D_{3h\bar{\sigma}}\bar{\tau})\bar{\theta}}$ -column and the $\tilde{B}_{(D_{3h\bar{\sigma}}\bar{\tau})\bar{\theta}}$ -column. It should be noted, however, that the RS -stereoisomeric group, for example, results in the formation of $(\mathbf{3}\ \bar{\mathbf{3}})_I$, $(\mathbf{5})_{IV}$, and $(\mathbf{7})_{IV}$ for the partition $[\bar{\theta}]_3$, while the stereoisomeric group results in the formation of $\langle \mathbf{3}\ \bar{\mathbf{3}} \rangle$, $\langle \mathbf{5} \rangle$, and $\langle \mathbf{7} \rangle$ for the partition $[\bar{\theta}]_3$. In this comparison, a pair of parentheses represents a set of RS -stereoisomers, while a pair of angle brackets represents a set of stereoisomers.

All of the values in the $B_{(S_{\sigma\bar{\tau}}^{[6]})\bar{\theta}}$ -column of Table 2 are found to be 1. This means that the isoskeletal group $S_{\sigma\bar{\tau}}^{[6]}$ bundles all of the prismane derivatives with a specific partition $([\bar{\theta}]_1-[\bar{\theta}]_{11})$ into one set of isoskeletonomers. This result can be understood on the basis of the property of the symmetric group $S^{[6]}$ (for defining the isoskeletal group $S_{\sigma\bar{\tau}}^{[6]}$) which contains all permutations concerning the numbers 1 to 6 ($6! = 720$). Note that the 60 transversals appearing in Eq. 10 have been selected from the elements of $S^{[6]}$.

The steps of the group hierarchy described above are consistent with the scheme represented by Eq. 8. They are accumulated to give the following scheme:

$$\{ \langle \langle (\mathbf{3}\ \bar{\mathbf{3}})_I \rangle \rangle \langle \langle (\mathbf{5})_{IV} \rangle \rangle \langle \langle (\mathbf{7})_{IV} \rangle \rangle \}. \quad (31)$$

According to a previous proposal of the author (Fujita) [31,32], the compound numbers in the scheme represented by Eq. 31 are replaced by the respective structural formulas to give an isomer-classification diagram shown in Figure 4.

In Figure 4 as well as Eq. 31, pairs of various brackets are used in a nested fashion: a pair of braces $\{\dots\}$ to show an equivalence class of isoskeletonomers under the isoskeletal

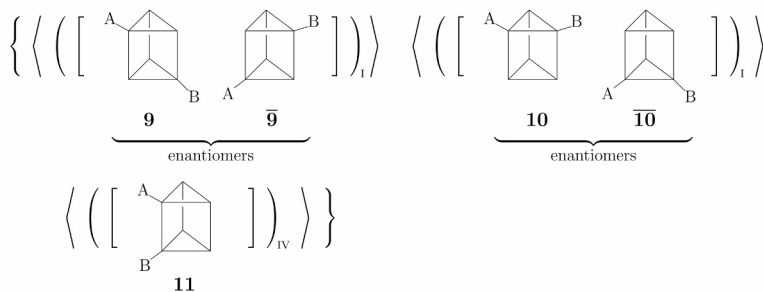


Figure 5. Isomer-classification diagram for prismanes with the composition H⁴AB.

group $\mathbf{S}_{\sigma\hat{T}}^{[6]}$; a pair of angle brackets $\langle \dots \rangle$ to show an equivalence class of stereoisomers under the stereoisomeric group, which is isomorphic to the RS -stereoisomeric group $\mathbf{D}_{3h\sigma\hat{T}}$; a pair of parentheses $(\dots)_{I,IV}$ to show a quadruplet of RS -stereoisomers as an equivalence class under the RS -stereoisomeric group $\mathbf{D}_{3h\sigma\hat{T}}$; a pair of square brackets $[\dots]$ to show a pair of (self-)enantiomers as an equivalence class under the point group \mathbf{D}_{3h} ; and each prismane derivative without such brackets to show as a single-membered equivalence class under the chiral point group \mathbf{D}_3 .

As for enantiomerism under the point group \mathbf{D}_{3h} , the chiral derivative **3** (or $\bar{\mathbf{3}}$) belongs to the point group \mathbf{C}_2 ; the achiral derivative **5** belongs to the point group \mathbf{C}_s ; and the other achiral derivative **7** belongs to the point group \mathbf{C}_{2v} . These point groups are the subgroups of the point group \mathbf{D}_{3h} . This fact can be confirmed by referring to the symmetry-itemized enumeration based on Fujita's USCI approach, which has been reported previously (Table 1 of [15]).

Let us next examine the values shown in the $[\check{\theta}]_4$ -row of Table 2, which can be discussed in a similar way to the above discussions on the $[\check{\theta}]_3$ -row. Thereby, we are able to construct an isomer-classification diagram, as shown in Figure 5.

The value 1 at the intersection between $[\check{\theta}]_4$ -row and the $B_{(\mathbf{S}_{\sigma\hat{T}}^{[6]})\check{\theta}}$ -column of Table 2 is consistent with one pair of braces appearing in Figure 5. Thus, there are one equivalence class of isoskeletomers under the action of the isoskeletal group $\mathbf{S}_{\sigma\hat{T}}^{[6]}$. The value 3 at the intersection between $[\check{\theta}]_4$ -row and the $\tilde{B}_{(\mathbf{D}_{3h\sigma\hat{T}})\check{\theta}}$ -column is consistent with three pairs of angle brackets appearing in Figure 5. Thus, there are three equivalence classes of stereoisomers under the action of the stereoisomeric group, which is isomorphic to the RS -stereoisomeric group $\mathbf{D}_{3h\sigma\hat{T}}$. The value 3 at the intersection between $[\check{\theta}]_4$ -row and the

$B_{(D_{3h\bar{\sigma}\bar{\tau}})\bar{\theta}}$ -column is consistent with three pairs of parentheses appearing in Figure 5. Thus, there are three equivalence classes of *RS*-stereoisomers under *RS*-stereoisomeric group $D_{3h\bar{\sigma}\bar{\tau}}$. Among them, the two pairs of parentheses correspond to type-I stereoisograms, while the one pair of parentheses correspond to a type-IV stereoisogram. The value 3 at the intersection between $[\bar{\theta}]_4$ -row and the $B_{(D_{3h})\bar{\theta}}$ -column is consistent with three pairs of square brackets appearing in Figure 5. Thus, there are three equivalence classes of (self-)enantiomers under the point group D_{3h} , i.e., two pairs of enantiomers ($[9\ \bar{9}]$ and $[10\ \bar{10}]$) and one pair of self-enantiomers ($[11]$, an achiral derivative). The value 5 at the intersection between $[\bar{\theta}]_4$ -row and the $T_{(D_3)\bar{\theta}}$ -column is supported by the presence of five prismane derivatives with the composition H^4AB . These five prismane derivatives, each of which is a single-membered equivalence class under D_3 , are inequivalent to one another under D_3 .

The prismane derivatives shown in Figure 5 belong to the subgroups of the point group D_{3h} . Thus, the chiral derivative **9** (or $\bar{9}$) belongs to the point group C_1 ($\subset D_{3h}$); the other chiral derivative **10** (or $\bar{10}$) belongs to the point group C_1 ($\subset D_{3h}$); and the achiral derivative **11** belongs to the point group C_s ($\subset D_{3h}$). This fact can be confirmed by referring to the symmetry-itemized enumeration based on Fujita's USCI approach, which has been reported previously (Table 1 of [15]).

3.4.3 Prismane derivatives with achiral and chiral proligands

The enumeration results of prismane derivatives with achiral and chiral proligands are collected in Tables 3 (the partitions $[\bar{\theta}]_{12}$ - $[\bar{\theta}]_{39}$) and 4 (the partitions $[\bar{\theta}]_{40}$ - $[\bar{\theta}]_{55}$). For the meaning of the partitions, see Eq. 23.

Let us examine prismane derivatives with the composition $H^4\bar{p}^2$ by referring to the $[\bar{\theta}]_{13}$ -row of Table 3. The isomer-classification diagram of these prismane derivatives is shown in Figure 6. Because the proligands p and \bar{p} selected from L_{3D} (Eq. 12) are differentiated during 3D enumeration under D_3 , D_{3h} , and $D_{3h\bar{\sigma}\bar{\tau}}$ (cf. the set of ligand-inventory functions represented by Eqs. 16–18), the composition $H^4\bar{p}^2$ corresponds to a set of the compositions H^4p^2 , $H^4\bar{p}^2$, and $H^4p\bar{p}$ without degeneration. On the other hand, the proligands p and \bar{p} degenerate into a single graph \bar{p} during 2D (graph) enumeration, although the same group $D_{3h\bar{\sigma}\bar{\tau}}$ is used to treat stereoisomerism (2D) as well as *RS*-stereoisomerism (3D). The degeneration of the compositions H^4p^2 , $H^4\bar{p}^2$, and $H^4p\bar{p}$ into a single composition $H^4\bar{p}^2$ is treated by the single ligand-inventory function represented by Eq. 25), which

Table 3. Hierarchical Enumeration of Cyclopropane Derivatives with Achiral and Chiral Proligands (Part 1)

| partition | numbers of prismane derivatives under respective groups | | | | |
|--|--|--|---|---|---|
| | $T_{(D_3)\bar{\theta}}$ (Eq. 19) | $B_{(D_{3h})\bar{\theta}}$ (Eq. 20) | $B_{(D_{3h,\bar{\sigma}})\bar{\theta}}$ (Eq. 21) | $\tilde{B}_{(D_{3h,\bar{\sigma}})\bar{\theta}}$ (Eq. 26) | $B_{(S_6^{\{6\}})\bar{\theta}}$ (Eq. 27) |
| | Eqs. 16-18 | | | Eq. 25 | |
| $[\dot{\theta}]_{12} = [5, 0, 0, 0, 0, 0, 1, 0, 0, 0, 0, 0]$ | 2 | 1 | 1 | 1 | 1 |
| $[\dot{\theta}]_{13} = [4, 0, 0, 0, 0, 0, 2, 0, 0, 0, 0, 0]$ | 13 | 8 | 6 | 3 | 1 |
| $[\dot{\theta}]_{14} = [4, 1, 0, 0, 0, 0, 1, 0, 0, 0, 0, 0]$ | 10 | 5 | 3 | 3 | 1 |
| $[\dot{\theta}]_{15} = [4, 0, 0, 0, 0, 0, 1, 1, 0, 0, 0, 0]$ | 20 | 10 | 6 | 3 | 1 |
| $[\dot{\theta}]_{16} = [3, 0, 0, 0, 0, 0, 3, 0, 0, 0, 0, 0]$ | 28 | 14 | 9 | 3 | 1 |
| $[\dot{\theta}]_{17} = [3, 2, 0, 0, 0, 0, 1, 0, 0, 0, 0, 0]$ | 20 | 10 | 6 | 6 | 1 |
| $[\dot{\theta}]_{18} = [3, 1, 0, 0, 0, 0, 2, 0, 0, 0, 0, 0]$ | 40 | 22 | 12 | 6 | 1 |
| $[\dot{\theta}]_{19} = [3, 0, 0, 0, 0, 0, 2, 1, 0, 0, 0, 0]$ | 80 | 40 | 22 | 6 | 1 |
| $[\dot{\theta}]_{20} = [3, 1, 1, 0, 0, 0, 1, 0, 0, 0, 0, 0]$ | 40 | 20 | 10 | 10 | 1 |
| $[\dot{\theta}]_{21} = [3, 1, 0, 0, 0, 0, 1, 1, 0, 0, 0, 0]$ | 80 | 40 | 20 | 10 | 1 |
| $[\dot{\theta}]_{22} = [3, 0, 0, 0, 0, 0, 1, 1, 1, 0, 0, 0]$ | 160 | 80 | 40 | 10 | 1 |
| $[\dot{\theta}]_{23} = [2, 2, 0, 0, 0, 0, 2, 0, 0, 0, 0, 0]$ | 66 | 36 | 22 | 11 | 1 |
| $[\dot{\theta}]_{24} = [2, 0, 0, 0, 0, 0, 2, 2, 0, 0, 0, 0]$ | 252 | 130 | 74 | 11 | 1 |
| $[\dot{\theta}]_{25} = [2, 2, 1, 0, 0, 0, 1, 0, 0, 0, 0, 0]$ | 60 | 30 | 16 | 16 | 1 |
| $[\dot{\theta}]_{26} = [2, 2, 0, 0, 0, 0, 1, 1, 0, 0, 0, 0]$ | 120 | 60 | 32 | 16 | 1 |
| $[\dot{\theta}]_{27} = [2, 0, 0, 0, 0, 0, 2, 1, 1, 0, 0, 0]$ | 480 | 240 | 124 | 16 | 1 |
| $[\dot{\theta}]_{28} = [2, 1, 1, 0, 0, 0, 2, 0, 0, 0, 0, 0]$ | 120 | 62 | 32 | 16 | 1 |
| $[\dot{\theta}]_{29} = [2, 1, 0, 0, 0, 0, 2, 1, 0, 0, 0, 0]$ | 240 | 120 | 62 | 16 | 1 |
| $[\dot{\theta}]_{30} = [2, 1, 1, 1, 0, 0, 1, 0, 0, 0, 0, 0]$ | 120 | 60 | 30 | 30 | 1 |
| $[\dot{\theta}]_{31} = [2, 1, 1, 0, 0, 0, 1, 1, 0, 0, 0, 0]$ | 240 | 120 | 60 | 30 | 1 |
| $[\dot{\theta}]_{32} = [2, 1, 0, 0, 0, 0, 1, 1, 1, 0, 0, 0]$ | 480 | 240 | 120 | 30 | 1 |
| $[\dot{\theta}]_{33} = [2, 0, 0, 0, 0, 0, 1, 1, 1, 1, 0, 0]$ | 960 | 480 | 240 | 30 | 1 |
| $[\dot{\theta}]_{34} = [1, 1, 1, 1, 1, 1, 0, 0, 0, 0, 0, 0]$ | 120 | 60 | 60 | 60 | 1 |
| $[\dot{\theta}]_{35} = [1, 1, 1, 1, 1, 0, 1, 0, 0, 0, 0, 0]$ | 240 | 120 | 60 | 60 | 1 |
| $[\dot{\theta}]_{36} = [1, 1, 1, 1, 0, 0, 1, 1, 0, 0, 0, 0]$ | 480 | 240 | 120 | 60 | 1 |
| $[\dot{\theta}]_{37} = [1, 1, 1, 0, 0, 0, 1, 1, 1, 0, 0, 0]$ | 960 | 480 | 240 | 60 | 1 |
| $[\dot{\theta}]_{38} = [1, 1, 0, 0, 0, 0, 1, 1, 1, 1, 0, 0]$ | 1920 | 960 | 480 | 60 | 1 |
| $[\dot{\theta}]_{39} = [1, 0, 0, 0, 0, 0, 1, 1, 1, 1, 1, 0]$ | 3840 | 1920 | 960 | 60 | 1 |

Table 4. Hierarchical Enumeration of Cyclopropane Derivatives with Achiral and Chiral Proligands (Part 2)

| partition | numbers of prismane derivatives under respective groups | | | | |
|--|--|--------------------------------------|---|---|---|
| | $T_{(\mathbf{D}_3)\ddot{\theta}}$ | $B_{(\mathbf{D}_{3h})\ddot{\theta}}$ | $B_{(\mathbf{D}_{3h\bar{\sigma}\hat{T}})\ddot{\theta}}$ | $\tilde{B}_{(\mathbf{D}_{3h\bar{\sigma}\hat{T}})\ddot{\theta}}$ | $B_{(\mathbf{S}_{\sigma\hat{T}}^{[6]})\ddot{\theta}}$ |
| | (Eq. 19) | (Eq. 20) | (Eq. 21) | (Eq. 26) | (Eq. 27) |
| | Eqs. 16–18 | | | Eq. 25 | |
| $[\dot{\theta}]_{40} = [1, 0, 0, 0, 0, 0, 5, 0, 0, 0, 0, 0]$ | 32 | 16 | 10 | 1 | 1 |
| $[\dot{\theta}]_{41} = [2, 0, 0, 0, 0, 0, 4, 0, 0, 0, 0, 0]$ | 46 | 25 | 17 | 3 | 1 |
| $[\dot{\theta}]_{42} = [1, 0, 0, 0, 0, 0, 4, 1, 0, 0, 0, 0]$ | 160 | 80 | 42 | 3 | 1 |
| $[\dot{\theta}]_{43} = [1, 1, 0, 0, 0, 0, 4, 0, 0, 0, 0, 0]$ | 80 | 42 | 22 | 3 | 1 |
| $[\dot{\theta}]_{44} = [1, 0, 0, 0, 0, 0, 3, 2, 0, 0, 0, 0]$ | 320 | 160 | 84 | 6 | 1 |
| $[\dot{\theta}]_{45} = [2, 0, 0, 0, 0, 0, 3, 1, 0, 0, 0, 0]$ | 160 | 80 | 44 | 6 | 1 |
| $[\dot{\theta}]_{46} = [2, 1, 0, 0, 0, 0, 3, 0, 0, 0, 0, 0]$ | 80 | 40 | 22 | 6 | 1 |
| $[\dot{\theta}]_{47} = [1, 0, 0, 0, 0, 0, 3, 1, 1, 0, 0, 0]$ | 640 | 320 | 160 | 10 | 1 |
| $[\dot{\theta}]_{48} = [1, 1, 0, 0, 0, 0, 3, 1, 0, 0, 0, 0]$ | 320 | 160 | 80 | 10 | 1 |
| $[\dot{\theta}]_{49} = [1, 1, 1, 0, 0, 0, 3, 0, 0, 0, 0, 0]$ | 160 | 80 | 40 | 10 | 1 |
| $[\dot{\theta}]_{50} = [1, 0, 0, 0, 0, 0, 2, 2, 1, 0, 0, 0]$ | 960 | 480 | 244 | 16 | 1 |
| $[\dot{\theta}]_{51} = [1, 1, 0, 0, 0, 0, 2, 2, 0, 0, 0, 0]$ | 480 | 244 | 124 | 16 | 1 |
| $[\dot{\theta}]_{52} = [1, 0, 0, 0, 0, 0, 2, 1, 1, 1, 0, 0]$ | 1920 | 960 | 480 | 30 | 1 |
| $[\dot{\theta}]_{53} = [1, 1, 0, 0, 0, 0, 2, 1, 1, 0, 0, 0]$ | 960 | 480 | 240 | 30 | 1 |
| $[\dot{\theta}]_{54} = [1, 1, 1, 0, 0, 0, 2, 1, 0, 0, 0, 0]$ | 480 | 240 | 120 | 30 | 1 |
| $[\dot{\theta}]_{55} = [1, 1, 1, 1, 0, 0, 2, 0, 0, 0, 0, 0]$ | 240 | 120 | 60 | 30 | 1 |

is based on the 2D ligand inventory \mathbf{L}_{2D} of Eq. 24.

One pair of braces $\{\dots\}$ in Figure 6 indicates that all of the prismane derivatives are bundled into a single set of isoskeletomers under the action of the isoskeletal group $\mathbf{S}_{\sigma\hat{T}}^{[6]}$. This result is verified by the value 1 at the intersection of the $[\dot{\theta}]_{13}$ -row and the $B_{(\mathbf{S}_{\sigma\hat{T}}^{[6]})\ddot{\theta}}$ -column in Table 3.

Three pairs of angle brackets $\langle \dots \rangle$ in Figure 6 indicate the presence of three sets of stereoisomers, i.e., $\langle \mathbf{12} \ \overline{\mathbf{12}} \ \mathbf{13} \ \overline{\mathbf{13}} \ \mathbf{14} \ \overline{\mathbf{14}} \rangle$, $\langle \mathbf{15} \ \overline{\mathbf{15}} \ \mathbf{16} \ \mathbf{17} \rangle$, and $\langle \mathbf{18} \ \overline{\mathbf{18}} \ \mathbf{19} \rangle$. This result is verified by the value 3 at the intersection of the $[\dot{\theta}]_{13}$ -row and the $\tilde{B}_{(\mathbf{D}_{3h\bar{\sigma}\hat{T}})\ddot{\theta}}$ -column in Table 3.

Six pairs of parentheses $(\dots)_{I-V}$ in Figure 6 indicate the presence of six sets of *RS*-stereoisomers, i.e., $(\mathbf{12} \ \overline{\mathbf{12}} \ \mathbf{13} \ \overline{\mathbf{13}})_{III}$, $(\mathbf{14} \ \overline{\mathbf{14}})_{I}$, $(\mathbf{15} \ \overline{\mathbf{15}})_{II}$, $(\mathbf{16} \ \mathbf{17})_{V}$, $(\mathbf{18} \ \overline{\mathbf{18}})_{II}$, and $(\mathbf{19})_{IV}$, which are inequivalent to one another under the action of the *RS*-stereoisomeric group $\mathbf{D}_{3h\bar{\sigma}\hat{T}}$. This result is consistent with the value 6 at the intersection of the $[\dot{\theta}]_{13}$ -row and the $B_{(\mathbf{D}_{3h\bar{\sigma}\hat{T}})\ddot{\theta}}$ -column in Table 3.

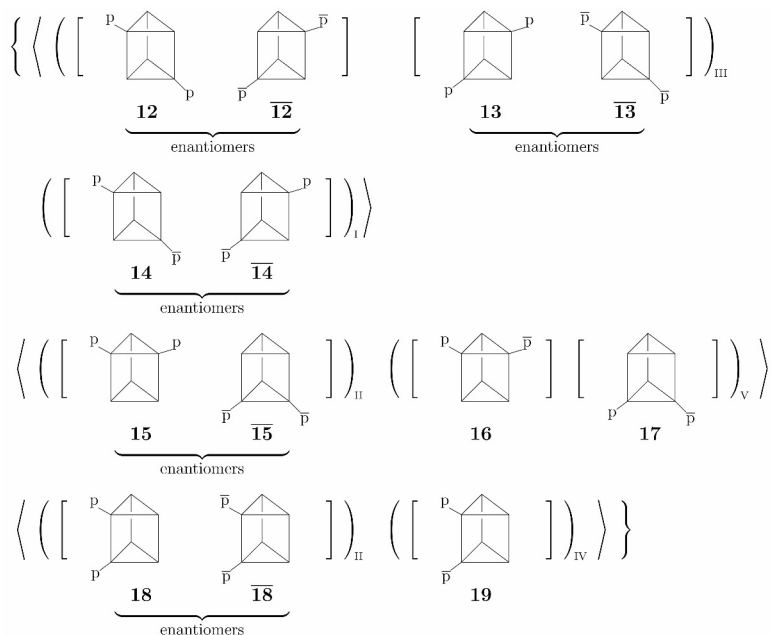


Figure 6. Isomer-classification diagram for prismane derivatives with the composition H^4p^2 (H^4p^2 , $H^4\bar{p}^2$, and $H^4p\bar{p}$).

Eight pairs of square brackets $[\dots]$ in Figure 6 indicate the presence of eight pairs of (self)-enantiomers, i.e., $[12 \bar{12}]$, $[13 \bar{13}]$, $[14 \bar{14}]$, $[15 \bar{15}]$, $[16]$, $[17]$, $[18 \bar{18}]$, and $[19]$, which are inequivalent to one another under the action of the point group D_{3h} . This result is consistent with the value 8 appearing at the intersection between the $[\check{\theta}]_{13}$ -row and the $B_{(D_{3h})\check{\theta}}$ -column in Table 3.

Finally, there appear 13 prismane derivatives in Figure 6, which are inequivalent under the point group D_3 . This result is consistent with the value 13 appearing at the last column of the $[\check{\theta}]_{13}$ -row.

The symmetry-itemized enumeration applied to prismane derivatives (Table 1 of [15]) indicates:

1. as prismanes with the composition $H^4p^2/H^4\bar{p}^2$, there are one pair of enantiomers belonging to C_1 ($[15 \bar{15}]$) and three pairs of enantiomers belonging to C_2 ($[12 \bar{12}]$, $[13 \bar{13}]$, and $[18 \bar{18}]$); and,
2. as prismanes with the composition $H^4p\bar{p}$, there are one pair of enantiomers belonging

to C_1 ($[14 \overline{14}]$), two achiral derivatives belonging to C_s ($[16]$, $[17]$), and one achiral derivatives belonging to C'_s ($[19]$).

The symmetry-itemized enumeration (Figures 5 and 6 of [15]) is consistent with the present result shown in Figure 6, when we pay attention to the action of the point group D_{3h} .

3.4.4 Prismane derivatives with chiral proligands

Hierarchical enumeration of prismane derivatives with chiral proligands and no achiral proligands is collected in Table 5, where the partitions $[\check{\theta}]_{56}$ - $[\check{\theta}]_{66}$ are taken into consideration.

Table 5. Hierarchical Enumeration of Cyclopropane Derivatives with Chiral Proligands

| partition | numbers of prismane derivatives under respective groups | | | | |
|--|--|--|--|--|--|
| | $T_{(D_3)\check{\theta}}$ (Eq. 19) | $B_{(D_{3h})\check{\theta}}$ (Eq. 20) | $B_{(D_{3h\bar{\sigma}\bar{\tau}})\check{\theta}}$ (Eq. 21) | $\tilde{B}_{(D_{3h\bar{\sigma}\bar{\tau}})\check{\theta}}$ (Eq. 26) | $B_{(S_{\sigma\bar{\tau}}^{[6]})\check{\theta}}$ (Eq. 27) |
| | Eqs. 16–18 | | | Eq. 25 | |
| $[\check{\theta}]_{56} = [0, 0, 0, 0, 0, 0, 6, 0, 0, 0, 0]$ | 16 | 9 | 8 | 1 | 1 |
| $[\check{\theta}]_{57} = [0, 0, 0, 0, 0, 0, 5, 1, 0, 0, 0]$ | 64 | 32 | 20 | 1 | 1 |
| $[\check{\theta}]_{58} = [0, 0, 0, 0, 0, 0, 4, 2, 0, 0, 0]$ | 172 | 88 | 54 | 3 | 1 |
| $[\check{\theta}]_{59} = [0, 0, 0, 0, 0, 0, 4, 1, 1, 0, 0]$ | 320 | 160 | 84 | 3 | 1 |
| $[\check{\theta}]_{60} = [0, 0, 0, 0, 0, 0, 3, 3, 0, 0, 0]$ | 216 | 108 | 62 | 3 | 1 |
| $[\check{\theta}]_{61} = [0, 0, 0, 0, 0, 0, 3, 2, 1, 0, 0]$ | 640 | 320 | 168 | 6 | 1 |
| $[\check{\theta}]_{62} = [0, 0, 0, 0, 0, 0, 3, 1, 1, 1, 0]$ | 1280 | 640 | 320 | 10 | 1 |
| $[\check{\theta}]_{63} = [0, 0, 0, 0, 0, 0, 2, 2, 2, 0, 0]$ | 984 | 496 | 268 | 11 | 1 |
| $[\check{\theta}]_{64} = [0, 0, 0, 0, 0, 0, 2, 2, 1, 1, 0]$ | 1920 | 960 | 488 | 16 | 1 |
| $[\check{\theta}]_{65} = [0, 0, 0, 0, 0, 0, 2, 1, 1, 1, 1, 0]$ | 3840 | 1920 | 960 | 30 | 1 |
| $[\check{\theta}]_{66} = [0, 0, 0, 0, 0, 0, 1, 1, 1, 1, 1, 1]$ | 7680 | 3840 | 1920 | 60 | 1 |

Let us examine the $[\check{\theta}]_{56}$ -row of Table 5, which shows the enumeration results of prismane derivatives with the composition \check{p}^6 . The corresponding isomer-classification diagram is shown in Figure 7. Note that the composition \check{p}^6 is itemized into p^6/\bar{p}^6 , $p^5\bar{p}/p\bar{p}^5$, $p^4\bar{p}^2/p^2\bar{p}^4$, and $p^3\bar{p}^3$.

The value 1 at the intersection between the $[\check{\theta}]_{56}$ -row and $B_{(S_{\sigma\bar{\tau}}^{[6]})\check{\theta}}$ -column indicates the presence of one equivalence class of isosketomers. This is illustrated by one pair of braces $\{\dots\}$, which surrounds all of the derivatives appearing in Figure 7.

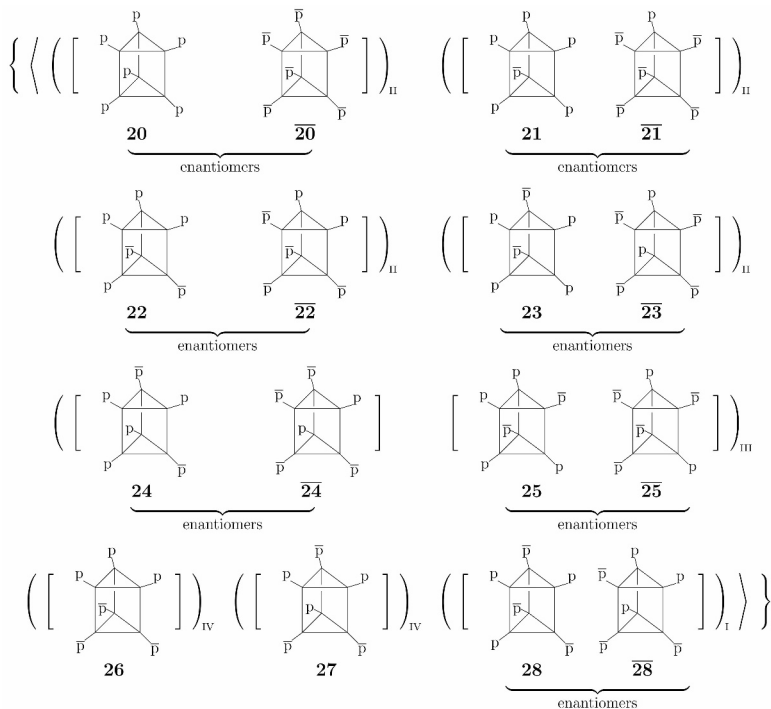


Figure 7. Isomer-classification diagram for prismane derivatives with the composition \bar{p}^6 (p^6/\bar{p}^6 , $p^5\bar{p}/p\bar{p}^5$, $p^4\bar{p}^2/p^2\bar{p}^4$, and $p^3\bar{p}^3$).

The value 1 at the intersection between the $[\bar{\theta}]_{56}$ -row and the $\tilde{B}_{(D_{3h\bar{\sigma}\hat{\tau}})\bar{\theta}}$ -column indicates the presence of one equivalence class of stereoisomers. This is illustrated by one pair of braces $\langle \dots \rangle$, which surrounds all of the derivatives appearing in Figure 7.

The value 8 at the intersection between the $[\bar{\theta}]_{56}$ -row and $B_{(D_{3h\bar{\sigma}\hat{\tau}})\bar{\theta}}$ -column indicates the presence of eight quadruplets of *RS*-stereoisomers, i.e., $(20\ 20)_{II}$, $(21\ 21)_{II}$, $(22\ 22)_{II}$, $(23\ 23)_{II}$, $(24\ 24\ 25\ 25)_{III}$, $(26)_{IV}$, $(27)_{IV}$, and $(28\ 28)_I$, each of which is an equivalence class under the action of the *RS*-stereoisomeric group $D_{3h\bar{\sigma}\hat{\tau}}$ and corresponds to a stereoisogram of type I, II, III, or IV, as shown by a subscript.

The value 9 at the intersection between the $[\bar{\theta}]_{56}$ -row and $B_{(D_{3h})\bar{\theta}}$ -column indicates the presence of nine pairs of (self)-enantiomers, i.e., $[20\ 20]$, $[21\ 21]$, $[22\ 22]$, $[23\ 23]$, $[24\ 24]$, $[25\ 25]$, $[26]$, $[27]$, and $[28\ 28]$, each of which is an equivalence class under the action of the point group D_{3h} .

Finally, there appear 16 prismane derivatives in Figure 7, the number of which is consistent with the value 16 at the intersection between the $[\theta]_{56}$ -row and $B_{(D_3)\bar{\theta}}$ -column. They are inequivalent under the chiral point group D_3 .

The symmetry-itemized enumeration applied to prismane derivatives (Table 1 of [15]) has itemized the values calculated under the point group D_{3h} . Thus, the value 9 at the intersection between the $[\theta]_{56}$ -row and $B_{(D_{3h})\bar{\theta}}$ -column is itemized as follows:

1. for p^6/\bar{p}^6 , there appears one pair of enantiomers belonging to D_3 ($[20 \bar{20}]$);
2. for $p^5\bar{p}/p\bar{p}^5$, there appears one pair of enantiomers belonging to C_1 ($[21 \bar{21}]$);
3. for $p^4\bar{p}^2/p^2\bar{p}^4$, there appear one pair of enantiomers belonging to C_1 ($[22 \bar{22}]$) and three pairs of enantiomers belonging to C_2 ($[23 \bar{23}]$, $[24 \bar{24}]$, and $[25 \bar{25}]$); and
4. for $p^3\bar{p}^3$, there appear one pair of enantiomers belonging to C_1 ($[28 \bar{28}]$), one achiral derivative belonging to C_{3h} ($[26]$), and one achiral derivative belonging to C_s ($[27]$).

3.5 3D-based and 2D-based enumerations

3.5.1 Comparison between prismane derivatives and cyclopropane derivatives

From the viewpoint of rigid 3D skeletons, the prismane skeleton **1** of ligancy 6 belongs to the point group D_{3h} and the *RS*-stereoisomeric group $D_{3h\bar{\sigma}\bar{\tau}}$, just as a cyclopropane skeleton of ligancy 6 (Part I of this series) belongs to the point group D_{3h} and the *RS*-stereoisomeric group $D_{3h\bar{\sigma}\bar{\tau}}$. It follows that the numbers of prismane derivatives in the $T_{(D_3)\bar{\theta}}$ -columns, the $B_{(D_{3h})\bar{\theta}}$ -columns, and the $B_{(D_{3h\bar{\sigma}\bar{\tau})\bar{\theta}}$ -columns of Tables 2–5 are equal to the numbers of cyclopropane derivatives in the $T_{(D_3)\bar{\theta}}$ -columns, the $B_{(D_{3h})\bar{\theta}}$ -columns, and the $B_{(D_{3h\bar{\sigma}\bar{\tau})\bar{\theta}}$ -columns of the corresponding tables reported in Part I of this series.

On the other hand, the prismane skeleton **1** does not undergo epimerization, whereas the cyclopropane skeleton can epimerize at each ring carbon atom. This means that the stereoisomeric group for the prismane skeleton is determined to be $D_{3h\bar{\sigma}\bar{\tau}}$ (order 24, the same as the *RS*-stereoisomeric group), while the stereoisomeric group for the cyclopropane skeleton is determined to be $\tilde{D}_{3h\bar{\sigma}\bar{\tau}}$ (order 96, different from the *RS*-stereoisomeric group). As a result, the numbers of sets of stereoisomers in the $\tilde{B}_{(D_{3h\bar{\sigma}\bar{\tau})\bar{\theta}}$ -columns for stereoisomerism of prismane derivatives may be different from the numbers of sets of stereoisomers in the $B_{(\tilde{D}_{3h\bar{\sigma}\bar{\tau})\bar{\theta}}$ -columns for stereoisomerism of cyclopropane derivatives. For

example, the number 3 at the intersection between the $[\tilde{\theta}]_3$ -row and the $\tilde{B}_{(\mathbf{D}_{3h\tilde{\sigma}\hat{\tau}})\tilde{\theta}}$ -column in Table 2 is different from the number 2 at the intersection between the $[\tilde{\theta}]_3$ -row and the $B_{(\tilde{\mathbf{D}}_{3h\tilde{\sigma}\hat{\tau}})\tilde{\theta}}$ -column in Table 2 of Part 1 of this series. The difference is confirmed by counting pairs of angle brackets $\langle \dots \rangle$ in their isomer-classification diagrams, i.e., Figure 4 of this article vs. Figure 4 of Part 1 of this series.

3.5.2 Pólya's enumeration method as a special case of the present approach

As discussed in Introduction, Pólya himself applied his enumeration method to the prismane skeleton **1** in Chapter 6 of [11]. Because reflections as well as rotations have been replaced by permutations, Pólya's discussion [11] is now concluded to be based on the *RS*-permutation group $\mathbf{D}_{3\tilde{\sigma}}$, which has been constructed to have no reflections, as found in Eq. 5. The cycle index reported on page 67 of [11] corresponds to the CI (without CF) of the *RS*-permutation group $\mathbf{D}_{3\tilde{\sigma}}$ ($\mathbf{D3s}$), i.e., $\text{CI}(\mathbf{D}_{3\tilde{\sigma}}, x_d)$ (CI_D3s), which is calculated by the GAP function `CycleIndex` as follows:

```
gap> D3s := Group([ (2,3)(5,6), (1,2)(4,5), (1,4)(2,5)(3,6) ]);
Group([ (2,3)(5,6), (1,2)(4,5), (1,4)(2,5)(3,6) ]);
gap> CI_D3s := CycleIndex(D3s);
1/12*x_1^6+1/4*x_1^2*x_2^2+1/3*x_2^3+1/6*x_3^2+1/6*x_6
```

It should be noted that the CI-CF (with CF!) of the *RS*-permutation group $\mathbf{D}_{3\tilde{\sigma}}$ ($\mathbf{D3s}$), i.e., CI-CF($\mathbf{D}_{3\tilde{\sigma}}, b_d$) (CICF_D3s), is calculated by using `CalcConjClassCICF` as follows:

```
gap> Read("c:/fujita0/fujita2017/prismane-GAP/Calc-GAP/CICFgenCC.gapfunc");
gap> D3s := Group([(2,3)(5,6), (1,2)(4,5), (1,4)(2,5)(3,6)]);;
gap> CICF_D3s := CalcConjClassCICF(D3s, 6, 6);
1/12*b_1^6+1/4*b_1^2*b_2^2+1/3*b_2^3+1/6*b_3^2+1/6*b_6
```

Compare the output of `CICF_D3s` with the output of `CI_D3s`. The CI without chirality fittingness (`CI_D3s`) can be alternatively obtained by substituting x_d (`x.d`) for the SI b_d (`b.d`) in the CI-CF (`CICF_D3s`), where the chirality fittingness (CF) is neglected by this substitution. This substitution is formally represented as follows:

$$\text{CI-CF}(\mathbf{D}_{3\tilde{\sigma}}, b_d) \Big|_{b_d=x_d} = \text{CI}(\mathbf{D}_{3\tilde{\sigma}}, x_d). \quad (32)$$

For the purpose of calculating the data of the $\tilde{B}_{(\mathbf{D}_{3h\tilde{\sigma}\hat{\tau}})\tilde{\theta}}$ -columns of the respective tables, the present approach adopts the CI-CF for the stereoisomeric group (the same as the CI-CF for the *RS*-stereoisomeric group $\mathbf{D}_{3h\tilde{\sigma}\hat{\tau}}$) listed in Table 1 ($\text{CI-CF}(\mathbf{D}_{3h\tilde{\sigma}\hat{\tau}}, \$_d)$, `CICF_D3hsI`) and the degenerated ligand-inventory function (Eq. 25). See Eq. 26. This treatment implies the intervention of a CI which is derived by substituting x_d (`x.d`) for each of the SIs (a_d , c_d , or b_d) in $\text{CI-CF}(\mathbf{D}_{3h\tilde{\sigma}\hat{\tau}}, \$_d)$ (`CICF_D3hsI` in Table 1). This substitution

is formally represented as follows:

$$\text{CI-CF}(\mathbf{D}_{3h\tilde{\sigma}\tilde{\tau}}, \mathbb{S}_d) \Big|_{\mathbb{S}_d=x_d} = \text{CI}(\mathbf{D}_{3\tilde{\sigma}}, x_d). \quad (33)$$

In fact, this substitution results in the derivation of a CI which is the same as the CI (CI_D3s) calculated by the above GAP code for the *RS*-permutation group $\mathbf{D}_{3\tilde{\sigma}}$ (D3s). In other words, the stereoisomeric group (the same as the *RS*-stereoisomeric group $\mathbf{D}_{3h\tilde{\sigma}\tilde{\tau}}$) is regarded as degenerating into the *RS*-permutation group $\mathbf{D}_{3\tilde{\sigma}}$ (D3s), so that the chirality fittingness (CF) due to the concept of sphericities [17] can be neglected. As a result, Pólya's enumeration method can be regarded as a special case of the present approach. Pólya's theorem has been concluded to be deficient in the concept of sphericities, as discussed in a review of the author (Fujita) [12].

4 Conclusion

Group hierarchy for characterizing a prismane skeleton with six substitution positions has been discussed by defining the point group \mathbf{D}_{3h} (order 12) for enantiomerism, the *RS*-stereoisomeric group $\mathbf{D}_{3h\tilde{\sigma}\tilde{\tau}}$ (order 24) for *RS*-stereoisomerism, the stereoisomeric group (the same as $\mathbf{D}_{3h\tilde{\sigma}\tilde{\tau}}$) for stereoisomerism, and the isoskeletal group $\mathbf{S}_{\sigma\tilde{\tau}}^{[6]}$ (order 1440) for isoskeletomerism. These groups are constructed successively according to the procedure described in Part 1 of this series, where the combined-permutation representations of degree 8 are used to calculate cycle indices with chirality fittingness (CI-CFs) after permutation representations of degree 6 are combined with the mirror-permutation representations of degree 2. A set of three ligand-inventory functions is defined to accomplish 3D enumerations, i.e., under the point groups \mathbf{D}_3 and \mathbf{D}_{3h} as well as under the *RS*-stereoisomeric group $\mathbf{D}_{3h\tilde{\sigma}\tilde{\tau}}$. On the other hand, a single ligand-inventory function is used to accomplish 2D enumerations, i.e., under the stereoisomeric group (the same as $\mathbf{D}_{3h\tilde{\sigma}\tilde{\tau}}$) and under the isoskeletal group $\mathbf{S}_{\sigma\tilde{\tau}}^{[6]}$. The enumeration results are discussed systematically in terms of isomer-classification diagrams.

References

- [1] A. Ladenburg, Bemerkungen zur aromatischen Theorie, *Chem. Ber.* **2** (1869) 140–142.
- [2] A. Kekulé, Ueber eignige Condensationsproducte des Aldehyds, *Justus Liebigs Ann. Chem.* **162** (1872) 77–124.
- [3] T. J. Katz, N. Acton, Synthesis of prismane, *J. Am. Chem. Soc.* **95** (1973) 2736–2739.
- [4] J. Dewar, On the oxidation of phenyl alcohol and a mechanical arrangement adapted to illustrate structure in the non-saturated hydrocarbons, *Proc. Royal Soc. Edinburgh* **6** (1867) 82–86.
- [5] A. J. Ihde, *The Development of Modern Chemistry*, Dover, New York, 1984.
- [6] G. Pólya, Un problème combinatoire général sur les groupes de permutations et le calcul du nombre des isomères des composés organiques, *Compt. Rend.* **201** (1935) 1167–1169.
- [7] G. Pólya, Tabelle der Isomerenzahlen für die einfacheren Derivate einiger cyclischen Stammkörper, *Helv. Chim. Acta* **19** (1936) 22–24.
- [8] G. Pólya, Algebraische Berechnung der Anzahl der Isomeren einiger organischer Verbindungen, *Z. Kristal. A* **93** (1936) 415–443.
- [9] G. Pólya, Kombinatorische Anzahlbestimmungen für Gruppen, Graphen und chemische Verbindungen, *Acta Math.* **68** (1937) 145–254.
- [10] G. Pólya, R. C. Read, *Combinatorial Enumeration of Groups, Graphs, and Chemical Compounds*, Springer, New York, 1987.
- [11] G. Pólya, R. E. Tarjan, D. R. Woods, *Notes on Introductory Combinatorics*, Birkhäuser, Boston, 1983.
- [12] S. Fujita, Sphericities of cycles. What Pólya's theorem is deficient in for stereoisomer enumeration, *Croat. Chem. Acta* **79** (2006) 411–427.
- [13] S. Fujita, Chirality fittingness of an orbit governed by a coset representation. Integration of point-group and permutation-group theories to treat local chirality and prochirality, *J. Am. Chem. Soc.* **112** (1990) 3390–3397.
- [14] S. Fujita, *Symmetry and Combinatorial Enumeration in Chemistry*, Springer, Berlin, 1991.

- [15] S. Fujita, Importance of the proligand–promolecule model in stereochemistry. I. The unit–subduced–cycle–index (USCI) approach to geometric features of prismane derivatives, *J. Math. Chem.* **50** (2012) 2202–2222.
- [16] S. Fujita, Graphs to chemical structures 1. Sphericity indices of cycles for stereochemical extension of Pólya’s theorem, *Theor. Chem. Acc.* **113** (2005) 73–79.
- [17] S. Fujita, *Combinatorial Enumeration of Graphs, Three-Dimensional Structures, and Chemical Compounds*, Univ. Kragujevac, Kragujevac, 2013.
- [18] S. Fujita, Stereogenicity revisited. Proposal of holantimers for comprehending the relationship between stereogenicity and chirality, *J. Org. Chem.* **69** (2004) 3158–3165.
- [19] S. Fujita, Pseudoasymmetry, stereogenicity, and the *RS*-nomenclature comprehended by the concepts of holantimers and stereoisograms, *Tetrahedron* **60** (2004) 11629–11638.
- [20] S. Fujita, *Mathematical Stereochemistry*, De Gruyter, Berlin, 2015.
- [21] S. Fujita, Importance of the proligand–promolecule model in stereochemistry. II. The stereoisogram approach to stereoisomeric features of prismane derivatives, *J. Math. Chem.* **50** (2012) 2168–2201.
- [22] S. Fujita, *Diagrammatical Approach to Molecular Symmetry and Enumeration of Stereoisomers*, Univ. Kragujevac, Kragujevac, 2007.
- [23] S. Fujita, Chirality and stereogenicity for square–planar complexes, *Helv. Chim. Acta* **85** (2002) 2440–2457.
- [24] S. Fujita, Sphericity governs both stereochemistry in a molecule and stereoisomerism among molecules, *Chem. Rec.* **2** (2002) 164–176.
- [25] <https://www.gap-system.org/>. GAP is the acronym of *Groups, Algorithms, Programming*.
- [26] S. Fujita, Computer–oriented representations of point groups and cycle indices with chirality fittingness (CI-CFs) calculated by the GAP system. Enumeration of three-dimensional structures of ligancy 4 by Fujita’s proligand method, *MATCH Commun. Math. Comput. Chem.* **76** (2016) 379–400.
- [27] S. Fujita, Computer–oriented representations of O_h -skeletons for supporting combinatorial enumeration by Fujita’s proligand method. GAP calculation of cycle indices with chirality fittingness (CI-CFs), *MATCH Commun. Math. Comput. Chem.* **77** (2017) 409–442.

- [28] S. Fujita, Computer-oriented representations of *RS*-stereoisomeric groups and cycle indices with chirality fittingness (CI-CFs) calculated by the GAP system. Enumeration of *RS*-stereoisomers by Fujita's proligand method, *MATCH Commun. Math. Comput. Chem.* **77** (2017) 443–478.
- [29] S. Fujita, Graphs to chemical structures 2. Extended sphericity indices of cycles for stereochemical extension of Pólya's coronas, *Theor. Chem. Acc.* **113** (2005) 80–86.
- [30] S. Fujita, Graphs to chemical structures 3. General theorems with the use of different sets of sphericity indices for combinatorial enumeration of nonrigid stereoisomers, *Theor. Chem. Acc.* **115** (2006) 37–53.
- [31] S. Fujita, Misleading classification of isomers and stereoisomers in organic chemistry, *Bull. Chem. Soc. Jpn.* **87** (2014) 1367–1378.
- [32] S. Fujita, Classification of stereoisomers. Flowcharts without and with the intermediate concept of *RS*-stereoisomers for mediating between enantiomers and stereoisomers, *Tetrahedron: Asymmetry* **27** (2016) 43–62.